Article

SOURCE DATA | TRANSPARENT PROCESS | OPEN ACCESS

THE EMBO JOURNAL

Infection and inflammation stimulate expansion of a CD74$^+$ Paneth cell subset to regulate disease progression

Iyshwarya Balasubramanian[1,†], Sheila Bandyopadhyay[1,†], Juan Flores[1], Jared Bianchi-Smak[1], Xiang Lin[2], Haoran Liu[2], Shengxiang Sun[3], Natasha B Golovchenko[4], Yue Liu[1], Dahui Wang[1], Radha Patel[1], Ivor Joseph[1], Panan Suntornsaratoon[5], Justin Vargas[6], Peter HR Green[6], Govind Bhagat[6,7], Stephen M Lagana[7], Wang Ying[8], Yi Zhang[8], Zhihan Wang[9], Wei Vivian Li[10], Sukhwinder Singh[11], Zhongren Zhou[12], George Kollias[13], Laura A Farr[14], Shannon N Moonah[14], Shiyan Yu[1], Zhi Wei[2], Edward M Bonder[1], Lanjing Zhang[1,15], Pawel R Kiela[16], Karen L Edelblum[4], Ronaldo Ferraris[5], Ta-Chiang Liu[3,*] & Nan Gao[1,*]

Abstract

Paneth cells (PCs), a specialized secretory cell type in the small intestine, are increasingly recognized as having an essential role in host responses to microbiome and environmental stresses. Whether and how commensal and pathogenic microbes modify PC composition to modulate inflammation remain unclear. Using newly developed PC-reporter mice under conventional and gnotobiotic conditions, we determined PC transcriptomic heterogeneity in response to commensal and invasive microbes at single cell level. Infection expands the pool of CD74$^+$ PCs, whose number correlates with auto or allogeneic inflammatory disease progressions in mice. Similar correlation was found in human inflammatory disease tissues. Infection-stimulated cytokines increase production of reactive oxygen species (ROS) and expression of a PC-specific mucosal pentraxin (Mptx2) in activated PCs. A PC-specific ablation of *MyD88* reduced CD74$^+$ PC population, thus ameliorating pathogen-induced systemic disease. A similar phenotype was also observed in mice lacking Mptx2. Thus, infection stimulates expansion of a PC subset that influences disease progression.

Keywords CD74; heterogeneity; lysozyme; Lyz1; Paneth cell
Subject Categories Chromatin, Transcription & Genomics; Immunology; Microbiology, Virology & Host Pathogen Interaction
DOI 10.15252/embj.2023113975 | Received 8 March 2023 | Revised 17 August 2023 | Accepted 18 August 2023 | Published online 18 September 2023
The EMBO Journal (2023) 42: e113975

Introduction

Paneth cells (PCs) are predominantly located in crypts of small intestine in healthy humans, increasing in abundance from duodenum to ileum. The number of PC decreases gradually from cecum to proximal colon, diminishing in the mid-transverse colon (Singh *et al*, 2020). Metaplastic PCs, when observed in distal colorectal

1 Department of Biological Sciences, Rutgers University, Newark, NJ, USA
2 Department of Computer Science, New Jersey Institute of Technology, Newark, NJ, USA
3 Department of Pathology and Immunology, Washington University School of Medicine, Saint Louis, MO, USA
4 Center for Immunity and Inflammation, Rutgers New Jersey Medical School, Newark, NJ, USA
5 Department of Pharmacology, Physiology & Neuroscience, Rutgers New Jersey Medical School, Newark, NJ, USA
6 Department of Medicine, Celiac Disease Center, Columbia University Irving Medical Center, New York, NY, USA
7 Department of Pathology and Cell Biology, Columbia University Irving Medical Center, New York, NY, USA
8 Hackensack Meridian Health Center for Discovery and Innovation, Nutley, NJ, USA
9 Department of Statistics, Rutgers University, New Brunswick, NJ, USA
10 Department of Biostatistics and Epidemiology, Rutgers University, New Brunswick, NJ, USA
11 Department of Pathology, Rutgers New Jersey Medical School, Newark, NJ, USA
12 Department of Pathology & Laboratory Medicine, Robert Wood Johnson Medical School, Rutgers University, New Brunswick, NJ, USA
13 Biomedical Sciences Research Centre, "Alexander Fleming", Vari, Greece
14 Division of Infectious Diseases and International Health, University of Virginia, Charlottesville, VA, USA
15 Department of Pathology, Penn Medicine Princeton Medical Center, Plainsboro, NJ, USA
16 Departments of Pediatrics and Immunology, and Daniel Cracchiolo Institute for Pediatric Autoimmune Disease Research, Steele Children's Research Center, The University of Arizona Health Sciences, Tucson, AZ, USA
*Corresponding author. Tel: +1 314 747 0343; E-mail: ta-chiang.liu@wustl.edu
**Corresponding author. Tel: +1 973 353 5523; E-mail: ngao@newark.rutgers.edu
†These authors contributed equally to this work

regions (Cunliffe *et al*, 2001; Cunliffe, 2003), are considered as pathologic evidence of prior injury in the context of inflammatory bowel disease (IBD). A well-defined PC defect characterized by aberrant intracellular granule morphology was found in Crohn's disease (CD; one of the two major IBD subtypes) patients bearing *ATG16L1 T300A*, or *NOD2* risk alleles (Cadwell *et al*, 2008; VanDussen *et al*, 2014). These characteristic PC granule phenotypes were used as surrogate markers for PC function (Cadwell *et al*, 2008). Increased frequency of "type I" PCs with "abnormal" granule patterns was first described in CD patients, where there are reduced lysozyme-positive granules, or lysozyme and α-defensin disperse into cytoplasm (Cadwell *et al*, 2008; Liu *et al*, 2014; VanDussen *et al*, 2014). We and others subsequently used these PC phenotypes as a prognostic indicator for the rapidness of CD recurrence after surgery (VanDussen *et al*, 2014; Khaloian *et al*, 2020), mucosal dysbiosis in pediatric CD (Liu *et al*, 2016), and impact of environmental risks such as cigarette smoking (Liu *et al*, 2018) or Western diet (Liu *et al*, 2021). Based on mouse experiments, it was proposed that ileal CD may represent a specific disorder of PCs (Adolph *et al*, 2013). Wehkamp and Stange (2020) hypothesized that PC abnormalities may play a key role in initiating inflammation in ileal and possibly ileocecal CD. However, there remain a scarcity of data that support these hypotheses.

A known function of mature PCs is the production of antimicrobial peptides (AMP) (Bevins & Salzman, 2011). Molecular abnormalities in secretory cargo packaging (Zhang *et al*, 2015), autophagy activation (Cadwell *et al*, 2008; Thachil *et al*, 2012; Spalinger *et al*, 2014), and unresolved endoplasmic reticulum (ER) stress (Adolph *et al*, 2013) have been hypothesized to impair PC function, affecting mucosal homeostasis and inflammation (Wehkamp & Stange, 2020). These uncovered mechanisms shed important lights on PC pathobiology but they were generally viewed as mechanism acting across the PC population. There is perhaps of a lacked appreciation of a potentially heterogeneous functionalities among this cell type. Abnormal PC secretion was widely believed as a contributing factor to CD pathology as reduced production of α-defensins was found in patients; however, increased or unchanged expression or production of other PC-enriched AMPs, such as REG3, lysozyme, angiogenin, β-defensin 3, phospholipase A2 were also observed in CD patients (Wehkamp *et al*, 2005b; Meisch *et al*, 2013; Begun *et al*, 2015; Rubio, 2015; reviewed in Wehkamp & Stange, 2020). Mice infected by *Salmonella typhimurium*, an enteric invasive pathogen, showed diminished PC lysozyme secretion (Salzman *et al*, 2003a). On the other hand, *Salmonella* also activated the lysozyme production through a secretory autophagy pathway in mouse PCs (Bel *et al*, 2017). Earlier studies attributed intestinal inflammation in part to an abnormal lysozyme secretion by PCs, while recent studies suggested that mice lacking PC lysozyme were protected from experimental colitis, while intestinal lysozyme overproduction was colitogenic (Yu *et al*, 2020). These studies suggest that it may be necessary to systemically examine the PC composition thereby understanding the potential diversity among various PC subsets.

Early study of mRNA expression of mouse *defensin* genes revealed a positional difference between proximal and distal small intestines, indicating a PC diversity along the longitudinal axis of small bowel (Darmoul & Ouellette, 1996). The single cell RNA profiling of whole mouse intestinal epithelium further illustrated the transcriptomic heterogenicity of individual cell types where PCs represented a minor subpopulation within the dataset (Haber *et al*, 2017). Recently, Kamioka *et al* (2022) defined a fucosyltransferase 2 (Fut2)-expressing ileum-enriched PC population that is regulated by IL22 and IL17 for development as part of the gut innate defense. From a pathology view, we and others have observed that IBD patients contain PCs of heterogenous phenotypes that include a notable normal-looking population, suggesting that not all PCs are pathogenic.

Here, we developed a new inducible mouse PC reporter, which enabled us to label, track, and genetically engineer PCs under conventional or gnotobiotic conditions. Through PC-specific single-cell (sc) RNA-Sequencing analysis, we established transcriptomic maps for PCs isolated from specific pathogen free (SPF), germ-free (GF), microbiota-transferred GF mice, and pathogen-infected mice. We found that GF mature PCs respond to microbiota colonization. Infection expands and activates a PC subset with signature transcriptome and biochemical markers. These PCs increase as disease progresses in $TNF^{\Delta ARE}$ ileitis and graft-versus-host disease (GvHD) mouse models, and can be detected in human tissues of inflammatory intestinal diseases. Genetic experiments ablating PC-specific MyD88 or mucosal pentraxin in mice demonstrated a notable impact on infection-stimulated immune cell recruitment, complement pathway activation, and progression of systemic disease.

Results

Paneth cells abnormalities are reported in CD (Tanaka *et al*, 2001; Simmonds *et al*, 2014) (Wehkamp *et al*, 2005b; Perminow *et al*, 2010; Adolph *et al*, 2013), ulcerative colitis (UC; the other major IBD subtype) (Tanaka *et al*, 2001; Bedini *et al*, 2014; Simmonds *et al*, 2014), celiac disease (Ward *et al*, 1979; Di Sabatino *et al*, 2008; Rubio, 2011), and GvHD (Fishbein *et al*, 2008; Levine *et al*, 2013; Kroemer *et al*, 2016). From a histopathological perspective, we first examined if PCs look heterogeneous in terms of biochemical expression of markers in biopsy tissues. We used α-defensin 5 (HD5), a widely accepted human PC marker (Jones & Bevins, 1992; Porter *et al*, 1997) to identify PCs. We examined their expression for REG3G, a c-type antimicrobial lectin (Arijs *et al*, 2009; Vaishnava *et al*, 2011; van Beelen Granlund *et al*, 2013) or MMP7, a matrix metalloproteinase that regulates defensin activity in mice (Wilson *et al*, 1995). From 22 IBDs involved tissues (16 CDs and 6 UCs) (Figs 1A and EV1A and B), 42 and 53% of PCs co-expressed HD5 and REG3G in CD and UC tissues, respectively (Fig 1B). Forty-two percent and 38% of PCs co-expressed HD5 and MMP7 in CD and UC tissues, respectively (Fig 1C and D). We also examined celiac disease ($n = 13$) and GvHD ($n = 10$) tissue biopsies and found that 85 and 49% of PCs co-expressed HD5 and MMP7 in celiac disease and GvHD, respectively (Fig 1C and E). These results suggest that human PCs have different protein expression profiles across population.

Paneth cells secret various antimicrobial proteins (Zasloff, 2002; Wehkamp *et al*, 2005a; Duerkop *et al*, 2009), but few studies have examined whether or not these proteins are secreted in identical fashions. Understanding that there is a change of gut microbiota in host transitioning from neonatal to adult stages, we temporally profiled four proteins (lysozyme, α-defensin 1, Mmp7, and Mptx2) known to be secreted by mouse PCs from neonatal and adult mice

(Figs 1F and G, and EV1D and E). Due to the limited fecal amount, antibody-based dot blots were done on fresh fecal lysates of pre-weaning C57BL6 pups (P10-15), adult, and aged mice (> 1-year). The abundance of fecal lysozyme did not change after weaning, α-defensin 1 increased (Figs 1G and EV1E). Both α-defensin 1 and lysozyme declined in aged animals, while Mmp7 and Mptx2, a PC mucosal pentraxin, declined after weaning but slightly elevated in aged mice (Figs 1F and G, and EV1D). These results suggest that PCs produce different products differently during the lifespan.

Development of Lyz1$^{3'UTR\text{-}CreER}$ mouse PC reporter

We developed an inducible *Lyz1*$^{3'UTR\text{-}CreER}$ mouse allele to genetically label and engineer PCs. Different from our previously reported *Lyz1* knockin mice that exhibit mosaic recombination (Yu *et al*, 2018), this new *Lyz1*$^{3'UTR\text{-}CreER}$ allele carrying an *IRES-CreER* cassette inserted at the 3′UTR of *Lyz1* locus (Fig 1H). After crossing to *Rosa26R-tdTomato* (tdT) reporter mice, founders with robust recombination in PCs were identified. After a single intraperitoneal (i.p.) injection of tamoxifen (TAM), the reporter was induced in PCs over time and reached near full recombination at 48 h ($n > 100$ mice, Figs 1I and EV1F). The reporter is specific to endogenous lysozyme-expressing or Mmp7-expressing PCs (Figs 1J and EV1G), and is equally expressed along the proximal to distal small intestines. PCs in enteroids developed from these mice can also be labeled by applying 4-OHT to the medium (Fig EV1H). Flow cytometry showed that tdT$^+$ cells co-expressed Cd24 (Fig EV1I), contained all EpCaM$^+$/Cd24$^+$ large cells (Fig EV1J). Image stream analysis demonstrated the cell surface Cd24 expression on the flow-sorted tdT$^+$ cells (Fig 1K).

Establishment of a deep PC-specific single-cell transcriptome

Haber *et al* (2017) generated a scRNA-Seq map of mouse small intestinal epithelium, where PCs represented a small portion of the entire epithelial cell populations (Haber *et al*, 2017). PCs in a human ileum scRNA-Seq dataset contained approximately 1.6% of the total transcriptome (Wang *et al*, 2020b). To gain depth into PC-specific transcriptome, including those low-copy or transcriptionally variable genes, we performed scRNA-Seq analysis on FACS-enriched tdT$^+$ PCs from *Lyz1*$^{3'UTR\text{-}CreER}$;Rosa26R-tdT reporter mice. Forty-eight hours after TAM injection, crypts were isolated (Fig 1L), digested into single cells (Fig 1M), and FACS sorted (Fig EV1I). We subjected a total of 6,626 duodenal and 6,893 ileal PCs isolated from the reporter mice on the same day to a droplet-based scRNA-Seq analysis (10× Genomics, Pleasanton, CA). These PCs showed 95.1% purity in tdT-expressing and 98.9% cellular viability determined by DAPI staining (Fig EV1K).

Seurat-based UMAP revealed three major compartments of these 13,519 PCs: PC progenitors expressing secretory precursor markers such as *Lgr5*, *Olfm4*, *Gkn3*, etc. (Buczacki *et al*, 2013) (Fig 1N), mature PCs expressing *Lyz1*, and various *Defa*, *Mptx2*, etc. (Fig 1O), and mature PCs expressing multiple long non-coding (lnc) RNAs (Fig 1P). *Atoh* is a master regulator of secretory cell types, including PCs (Kazanjian *et al*, 2010; Almohazey *et al*, 2017). *Atoh1*-expressing PCs are mapped next to the progenitor population in both duodenum and ileum (Figs 1Q and EV2A). Cell–cell correlation matrix (Fig 1R) revealed 12 sub-clusters that are resolved by unsupervised Seurat UMAP (Fig 1S). Each cluster has distinct transcriptional profiles (top 5 are shown per cluster, Fig 1T). This highly enriched population of PCs allowed us to obtain more total reads for any given genes (Fig EV2B), including low copy number genes, for example, microbial sensors (*MyD88*, *Tlr4*, and *Tlr5*) (Fig 1U and V), cytokine receptors (*Il17r*, *Il22r*, etc.) (Takahashi *et al*, 2008; Gaudino *et al*, 2021; He *et al*, 2022; Kamioka *et al*, 2022) (Fig EV2C–E), and CD-associated autophagy gene *Atg16l1* (Cadwell *et al*, 2008) (Fig EV2F). The smallest cluster of 80 cells (0.59% of total population) was identified as *Lyz1*$^+$/*Gzma*$^+$/*Cd45*$^+$/*Cd3*$^+$/*EpCAM*$^-$/*Mptx2*$^-$/*Muc2*$^-$ likely representing intraepithelial lymphocytes (Fig EV2G and H).

Gut commensal microbiome changes germ-free PC transcriptome

To understand how gut commensal microbiome regulates PC transcriptomic changes, we derived a germ free (GF) colony of these PC reporter mice through the US National Gnotobiotic Rodent Resource Center. Different founders from the rederivation were maintained to produce gnotobiotic lines of offspring. Injecting tamoxfen to adult GF PC reporter mice induced tdT expression as seen in specific pathogen free (SPF) reporter mice (Fig 2A), confirming that GF mice have PCs in the absence of microbiota (Kernbauer *et al*, 2014). We next performed total fecal microbiome transfer to these GF PC reporters. We collected cecum microbiota from wild type SPF C57BL/6 mice, resuspended the slurry in PBS under anaerobic condition, and transferred the microbiota through oral gavage. Successful transfer and colonization were validated by qPCR amplification of fecal bacterial 16S rRNA from the recipients (Fig EV3A). After 21 days of transplantation, sterile tamoxifen was administrated to exGF+B6M mice and littermate GF mice (separately housed to keep as GF controls). Live tdT$^+$ ileal PCs were isolated on the same day from GF and exGF+B6M mice and subjected to scRNA-Seq analysis (Fig 2B). UMAP showed that progenitor PCs from GF and microbiome-transferred mice shared similar transcriptome, while the mature PC populations differed from each other (Fig 2C). Trajectory analysis by the Slingshot (Street *et al*, 2018), which identifies lineages constructed a tree between these nodes, revealing two lineages (denoted as solid and dashed lines, Fig 2D). Both lineages started from progenitor clusters 0 and 3 (Fig 2E), which express *Olfm4* and *Lgr5* (Figs 2F and EV3B), and developed into mature cluster 1 (primarily GF) and cluster 2 (primarily exGF+B6M), respectively (Figs 2E and EV3C). The Slingshot trajectory constructed from GF only and exGF+B6M only PCs (Fig EV3D) suggested that microbiota transfer induced a change of preexisting mature GF PCs (cluster 1) into exGF+B6M PCs (cluster 2).

The two mature populations (cluster 1 and 2) are correlated in correlation analysis (Fig EV3E). Differentially expressed transcripts between cluster 1 (GF) and cluster 2 (exGF+B6M) PC populations (Fig 2G) include the most significantly elevated *Mptx2*, *Reg3g*, *AY761185*, and *Defa35* in exGF+B6M (Figs 2H, J and K, and EV3F and H). Jun, Fos, and MAPK signaling downstream genes, were reduced in exGF+B6M mature PCs (Figs 2G and I, and EV3G). No difference in the abundance of *Lyz1* transcript was found between cluster 1 (GF) and cluster 2 (exGF+B6M) (Fig 2L), suggesting that microbial colonization did not affect *Lyz1* expression. The two small clusters have enriched expression of *Enpep*, *Clec2h*, and *Chp2* (cluster 4) and *Dock10*, *St8sia4*, and *Ptprc* (cluster 5).

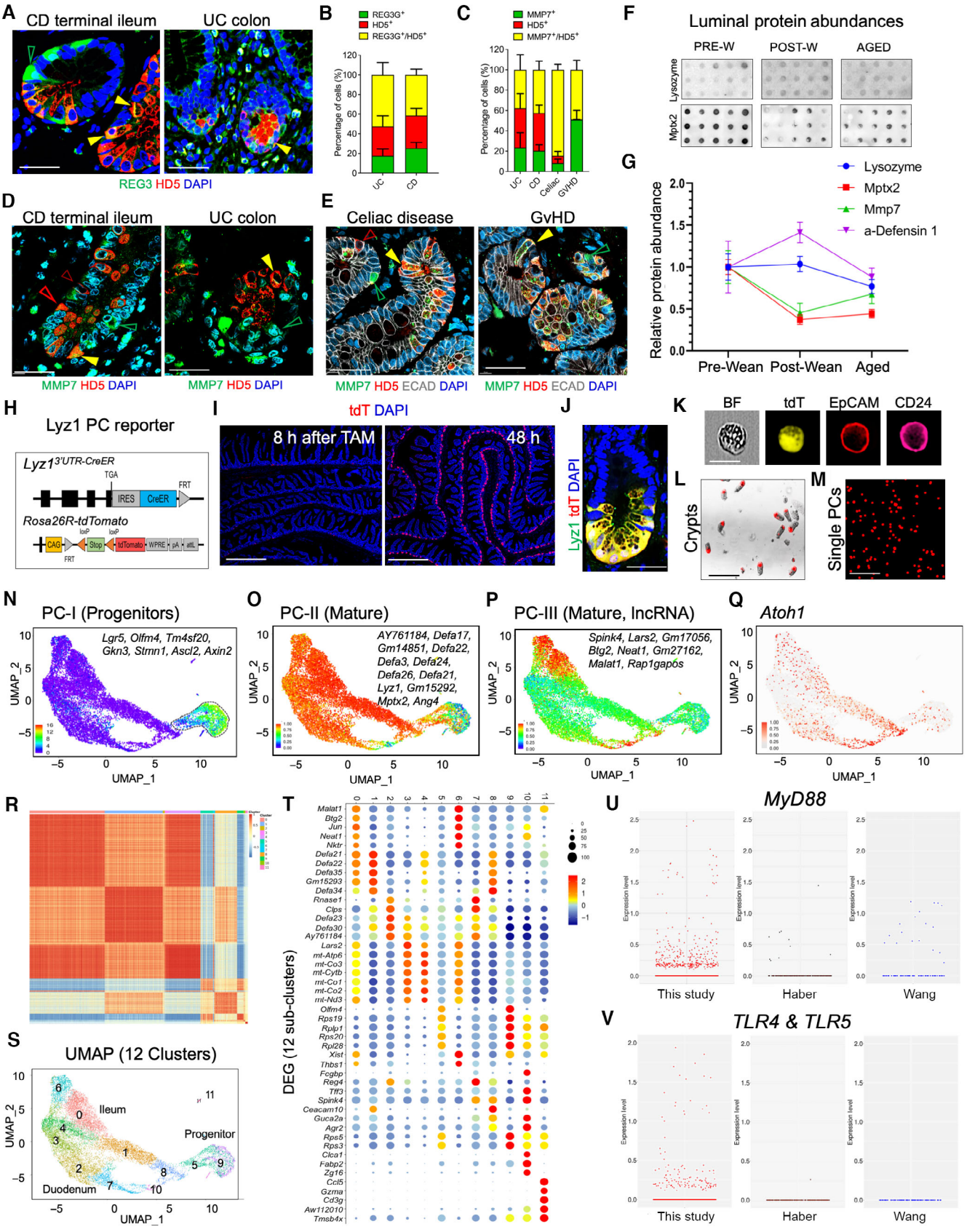

Figure 1.

Figure 1. Single cell transcriptomic profiling of Paneth cells isolated from PC reporter mice.

A Representative immunofluorescent analysis for human α-defensin 5 (HD5) and REG3G in human IBDs. Yellow arrows point to cells with co-staining of both proteins. Scale bars, 20 μm.
B Percentage of Paneth cells expressing only HD5, only REG3, or both proteins in 16 CD and 6 UC tissues.
C Percentage of Paneth cells expressing only HD5, only MMP7, or both proteins in CD (n = 21), UC (n = 15), celiac disease (n = 13), and GvHD (n = 10) tissues.
D Representative immunofluorescent analysis for HD5 and MMP7 in CD ileums and UC colons. Yellow arrows point to double positive cells; red and green arrows point to cells positive only for HD5 or MMP7, respectively. Scale bars, 20 μm.
E Representative immunofluorescent analysis for HD5, MMP7 and E-Cadherin in human celiac disease and GvHD intestinal tissues. Yellow arrows point to double positive cells; red and green arrows point to cells positive only for HD5 or MMP7, respectively. Scale bars, 20 μm.
F Mouse fecal pellets were collected from wild type mice of pre-weaning age (P10-15), 1-month old post-weaning young adults, and aged adults over 1-year old. 40-μg protein extract per sample was used for dot blotting analysis by lysozyme or Mptx2 antibodies. Columns represent different biological samples loaded in technical triplicates.
G Densitometry quantifications of dot blots for lysozyme, Mptx2, Mmp7, or α-defensin 1 from pre-weaning age (n = 5), 1-month old adults (n = 9), and aged mice (n = 11). Blots of Mmp7 and α-defensin 1 are shown in Fig EV1D and E. Error bars represent standard error of the mean (SEM).
H Schematic diagram of the newly developed Lyz1$^{3'UTR\text{-}IRES\text{-}CreER}$ inducible PC transgenic mice. After crossing to Rosa26R-tdTamato mice, the resulting mice are referred to as PC reporter.
I Lyz1$^{3'UTR\text{-}IRES\text{-}CreER}$; Rosa26R-tdTomato (PC reporter) mice were injected with a single dose of tamoxifen. 8, 24, and 48 h later, mice were sacrificed, and intestinal tissue sections were stained for tdTomato (red) and DAPI (blue). Scale bars, 200 μm.
J Representative PC reporter mouse small intestines were stained for tdT and endogenous lysozyme. Scale bars, 10 μm.
K Representative ImageStream analysis of FACS-sorted live single tdT$^+$ Paneth cells stained for EpCAM and CD24. Scale bars, 5 μm.
L Forty-eight hours after tamoxifen injection, live crypts were isolated from PC reporter mice, and visualized for the direct tdT fluorescence under epi-fluorescent microscope. Scale bars, 200 μm.
M Isolated crypts were digested to single cell suspension, which were visualized for direct tdT fluorescence under epi-fluorescent microscope. Scale bars, 200 μm.
N–P 10× Genomics scRNA-Seq and Seurat-based UMAP analysis of 13,519 duodenal and ileal Paneth cells. Marker genes identified three major populations corresponding to the PC progenitors (panel N), mature PCs (panel O), and a subset of mature PCs (panel P) with several enriched lncRNA. Gene sets were shown in individual graphs.
Q UMAP analysis of Atoh1-expressing Paneth cells.
R Cell–cell correlation matrix analysis shows 12 clusters.
S Seurat UMAP shows 12 unsupervised clusters.
T Top 5 differentially enriched genes of each cluster were shown in dot plots. Clusters 5 and 9 are PC progenitors. The smallest cluster (cluster 11) is a non-PC cluster.
U, V Comparison of the reads of *MyD88*, *TLR4*, and *TLR5* in PCs of this current PC-specific scRNA dataset, with scRNA sequencing dataset of mouse small intestinal epithelial cells (Haber), and human small intestine (Wang).

Source data are available online for this figure.

Immunostaining validated a limited number of Mptx2-expressing PCs in GF mouse ileum (Fig 2M). The number significantly increased in SPF mouse ileum (Fig 2M and N). In contrast, Lyz1-expressing PCs were slightly increased in SPF mice comparing to GF mice (Fig 2O and P). In addition, GF PCs contain clearly defined lysozyme-containing granules (Fig 2Q), suggesting that the commensal microbiome is dispensable for lysozyme granule formation in GF mouse PCs.

As above results suggested that a total gut commensal microbiota modulates the transcriptome of mature PC, we asked if different commensal bacterial species may differentially alter PC programs. *Lacticaseibacillus rhamnosus* is the world's most widely used probiotic species originally isolated from a healthy adult and with numerous perceived health benefits (Yan & Polk, 2002; Doron *et al*, 2005; Lebeer *et al*, 2008; Donato *et al*, 2010; Segers & Lebeer, 2014; Vong *et al*, 2014). *Ruminococcus gnavus* is an IBD-associated commensal bacterium (Png *et al*, 2010; Willing *et al*, 2010; Joossens *et al*, 2011; Hall *et al*, 2017; Nishino *et al*, 2018), which is sensitive to PC-derived lysozyme (Yu *et al*, 2020). Intrigued by their contrasting impacts on gut health, we therefore mono-associated GF mice (C57BL6, Taconic) with *L. rhamnosus* or *R. gnavus* (n = 5 for each group) for 3 weeks and compared their ileal PCs with GF mice that were gavaged with sterile PBS (n = 5). Compared to GF ileum (PBS control), *R. gnavus* mono-associated mice had an increased number of Mptx2-expressing ileal PCs, whereas *L. rhamnosus* mono-associated mice showed no difference compared to GF mice (Fig 2R and S). *R. gnavus* had insignificant effect on the number of Lyz1-expressing PCs, while *L. rhamnosus* diminished Lyz1-expressing PCs (Fig 2T and U). Interesting, *R. gnavus* moderately increased Lyz1-containing granules while *L. rhamnosus* reduced them in mono-associated mice (Fig 2V and W). Bulk RNA-Seq analysis of the terminal ileum of these mice suggested that *L. rhamnosus* globally suppressed PC transcripts, while *R. gnavus* increased *Mptx2*, *Reg3g*, *Atoh1* (Figs 2X and EV3I and J). These results suggested that gut microbiota and specific commensal microbes differentially modify PC transcriptomes and potentially their biological functions.

Enteric pathogenic bacteria activate a PC subset

Salmonella typhimurium infection in mice diminished PC lysozyme secretion (Salzman *et al*, 2003a), and activated secretory autophagy pathway for lysozyme secretion (Bel *et al*, 2017). To investigate if pathogens such as *Salmonella* may affect PC transcriptomic heterogeneity, we labeled PCs in reporter mice, and inoculated the mice with *S. typhimurium* (SL1344) (referred to as +SAL group) or PBS (−SAL group) (Fig 3A). Following the widely accepted procedure (Barthel *et al*, 2003), both groups were orally pretreated with streptomycin to increase infection susceptibility, and the only difference between +SAL and −SAL groups was *Salmonella* infection (Fig 3A). The tdT reporter was activated prior to infection, and tracked in labeled PCs after infection (Fig 3B). No proliferation of PCs was detected by PCNA staining (Fig 3B). scRNA profiling of +SAL and −SAL mouse ileal PCs isolated 4-day post-infection (4 d.p.i.) showed that the PC progenitor from both groups were clustered at proximity (Fig 3C–E). Within the +SAL PCs, a subpopulation with enriched expression of 49 transcripts was uncovered (top 9 shown

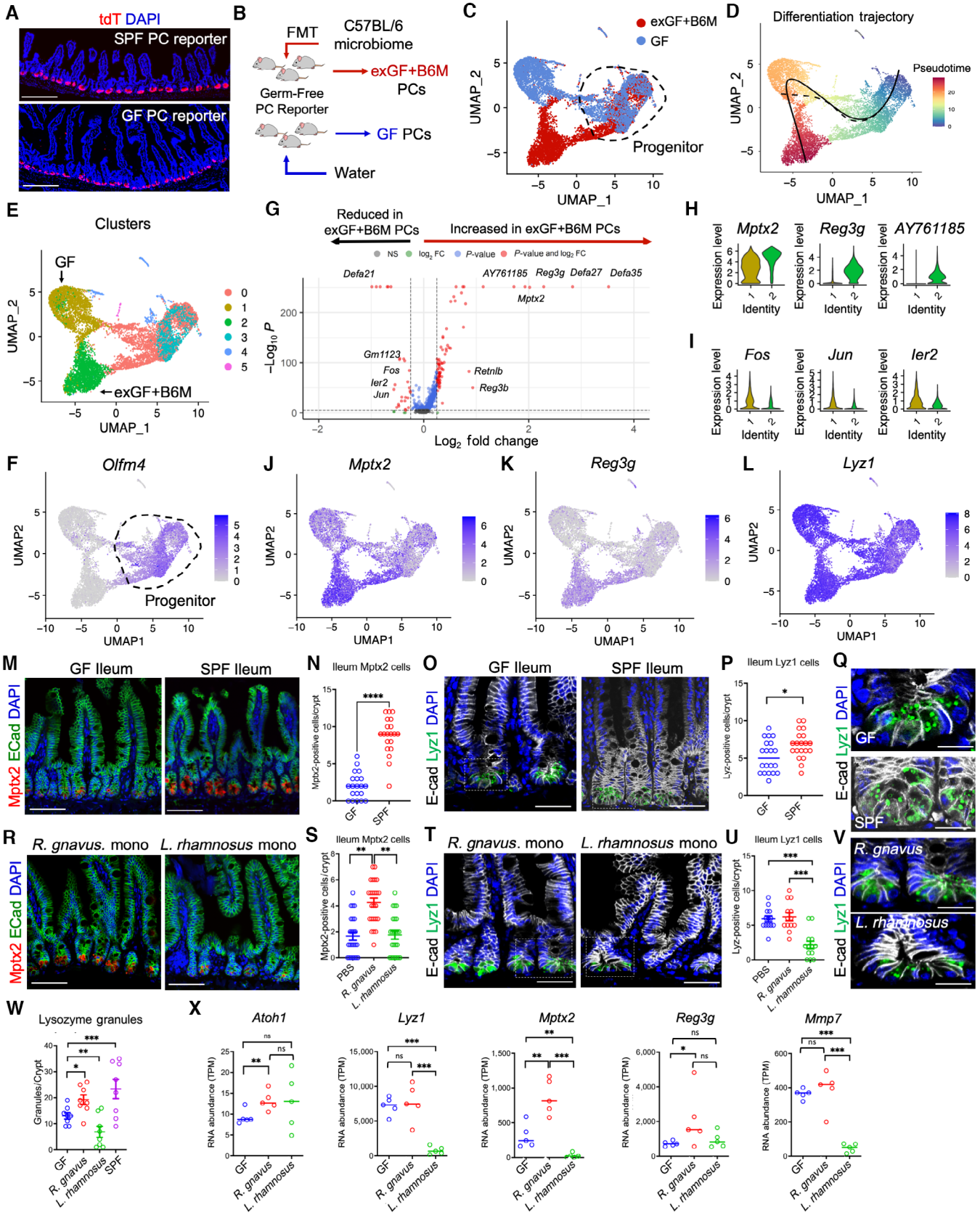

Figure 2.

Figure 2. Gut microbiota transfer in germ-free (GF) mice changes PC single cell transcriptome.

A A colony of PC reporter mice was re-derived into germ free. GF reporter mice were injected with sterile tamoxifen to activate the reporter and sacrificed at day 3. Representative GF and SPF reporter mouse ilea were imaged by confocal immunofluorescent analysis for tdT expression. Scale bars, 100 μm.

B GF PC reporter littermates were divided into two groups: one group was orally gavaged with freshly prepared C57BL/6 cecum microbiota (exGF+B6M) and the other group received water (kept as GF controls). After 3 weeks of colonization, mice were injected with sterile tamoxifen, and PCs were isolated from both groups for scRNA-seq analysis.

C UMAP shows ileal 5,224 and 5,646 PCs of GF (blue) and GF+B6M (red) conditions, respectively.

D Slingshot trajectory analysis revealed two lineages (denoted as dashed and solid lines), both of which started from PC progenitors (cluster 0 and 3). The first trajectory (dashed line) terminated at cluster 1 (primarily GF mature PCs) while the second (solid line) terminated at cluster 2 (primarily exGF+B6M mature PCs). The shown pseudotime variables represent the second lineage (solid line, exGF+B6M PCs). Note the cluster 1 contains a small number of exGF+B6M PCs (please see Fig EV3C).

E UMAP shows five unsupervised clusters.

F UMAP analysis of *Olfm4*$^+$ PC progenitors.

G Differential gene expression analysis comparing cluster 1 (primarily GF PCs) and cluster 2 (primarily exGF+B6M PCs) shown as a volcano plot. Top increased transcripts in cluster 2, include *Reg3g*, *Mptx2*, *Defa27*, *Defa35*, and *AY761185*.

H, I Violin plots show the top increased and decreased transcripts in cluster 1 versus cluster 2 PCs.

J–L UMAP analysis of PCs expressing *Mptx2*, *Reg3g*, and *Lyz1*.

M–P Immunofluorescent analysis for Mptx2 (M) or Lysozyme (O) in age matched GF and SPF mouse ileums. Numbers of cells positive for each marker protein were counted per crypt from approximately 100 crypts imaged from 20 to 25 independent microscopic fields from five mice per condition. Average values of individual field and unpaired *t*-test were reported in panel (N) for Mptx2 (****$P < 0.0001$) and panel (P) for lysozyme (*$P < 0.05$). Scale bars, 20 μm.

Q Representative high magnification images of lysozyme staining in GF and SPF ileal PCs. Scale bars, 10 μm.

R–U Immunofluorescent analysis for Mptx2 (R) or lysozyme (T) on ileum sections of GF mice mono-colonized with *R. gnavus* or *L. rhamnosus* for 21 days. Two experiments were performed for each mono-colonization. Cells positive for each protein marker per crypt were counted from different microscopic fields from five mice per condition. Average values of individual fields and one-way ANOVA test were reported in (S) and (U). GF mice gavaged with PBS were used as control. **$P < 0.01$; ***$P < 0.001$. Scale bars, 20 μm.

V Representative high magnification images of lysozyme staining in *R. gnavus* or *L. rhamnosus* monocolonized mouse ileal PCs. Scale bars, 10 μm.

W The number of lysozyme-containing granules per crypt were counted and averaged from each image of 2–3 high magnification images per condition. $n = 5$ mice for each condition. One-way ANOVA test was performed. *$P < 0.05$; **$P < 0.01$; ***$P < 0.001$.

X GF mice gavaged with PBS, monocolonized by *R. gnavus* or by *L. rhamnosus* ($n = 5$ mice for each condition) were sacrificed 21 days after colonization. Bulk RNA-Seq analysis were performed on total ileum RNA. Transcripts of *Atoh1*, *Lyz1*, *Mptx2*, *Reg3g*, and *Mmp7* per million reads were plotted with adjusted *P*-values from differential gene expression analysis for RNA-Seq tool in CLC genomics based on GLM model. *$P < 0.05$; **$P < 0.01$; ***$P < 0.001$.

Source data are available online for this figure.

in Figs 3F and EV4A). Among these genes, *Mmp7*, *Mptx2*, *Reg3g*, *Reg3b*, *Retnlb*, *Lypd8*, *Ifitm3* relate to antimicrobial functions, while *Gpx2* and *Gadd45g* regulates ROS activity (Chu *et al*, 2004) and DNA damage response (Ying *et al*, 2005), respectively. *Cd74* functions as the invariant chain of class II major histocompatibility complex (MHCII) for antigen presentation as well as the receptor for macrophage migration inhibitory factor (MIF). MIF stimulates Cd74 to regulate macrophage migration, inflammation (Collins *et al*, 1984; Volc-Platzer *et al*, 1984; Momburg *et al*, 1986), and wound healing (Stockinger *et al*, 1989; Lawrance *et al*, 2001; Borghese & Clanchy, 2011; Parikh *et al*, 2019; Farr *et al*, 2020a). These results suggest that *Salmonella* infection activated a PC subset with an inflammatory modulatory gene signature.

The *Cd74* transcripts were detected in SPF PC progenitors but scarcely in mature SPF, GF, exGF+B6M, or −SAL (with ABX) PCs (Figs 3F, EV2H, EV3H and EV4B–D), suggesting that mature *Cd74*-expressing PCs were primarily induced by infection. We conducted a model-based deep embedding for constrained clustering analysis (scDCC), based specifically on *Cd74*-expressing, to cluster SPF, −SAL (with ABX), and +SAL (with ABX) PCs using scRNA datasets. scDCC is a machine-learning algorithm recently developed by us to cluster cells with constraints from marker genes (Tian *et al*, 2021). Within +SAL PC population (green in Fig 3G), one of the *Cd74*-expressing clusters (circled in Fig 3H) was also enriched with *Mptx2* (Fig 3I) or *Gpx2* (Fig EV4E). Dot plots illustrated that *β defensin* 1 (*Defb1*) and multiple *Defa* genes were increased by *Salmonella* infection, whereas *Lyz1* was reduced upon infection (Figs 3J and EV4C and D), suggesting that infection differentially alters PC antimicrobial genes.

Different from antimicrobial genes, CD74 abundance appeared to be primarily induced by infection. We therefore examined CD74 expression *in vivo*, by using specific antibodies validated on *Cd74*$^{-/-}$ mouse tissues by immunostaining (Fig EV4E) and by flow cytometry (Fig EV4F). CD74-expressing PCs are rare in homeostasis, but could be identified in *Salmonella*-infected mouse ileum (Fig 3K). We quantified the number of Cd74$^+$ PCs by flow cytometry in whole ileal crypt epithelial cell populations. The percentage of tdT$^+$/CD74$^+$ PCs increased by 3.4-fold in +SAL mice comparing to −SAL controls (Fig 3L). In −SAL mice, the majority of CD74-expressing crypt epithelial cells were non-PCs; while after infection, 10–15% PCs became CD74-expressing (Fig 3M). We observed a 1.7-fold increase in tdT$^+$/CD74$^+$ PC population when TAM was injected after *Salmonella* inoculation, comparing to TAM injected before *Salmonella* infection (Fig 3N), suggesting that existing PCs as well as non-PCs (possibly the CD74$^+$ intestinal stem cells) (Biton *et al*, 2018) may give rise to CD74$^+$ PCs after infection. Image Stream analysis of tdT$^+$ +SAL PCs (representing 100–300 images each experiment) showed cell surface as well as cytoplasmic CD74 localizations (Fig 3O).

We validated the expansion of CD74$^+$ PCs in *Salmonella*-infected wild type C57BL/6 non-reporter mice using the CD24$^+$/EpCAM$^+$ gating strategy (Fig EV5A). *Salmonella* significantly increased the percentages of CD74$^+$/CD24$^+$/EpCAM$^+$ large PCs (Fig 3P and Q). Gating on all EpCAM$^+$ cells (Fig EV5D) showed a 2.54 ± 0.84-fold increase of CD74$^+$ non-PC epithelial cells upon infection, suggesting that expansion of CD74$^+$ PCs was part of a global IEC response to infection. The mouse genetic background has been known to influence PCs (Gulati *et al*, 2012). Expansion of CD74$^+$ PCs were also observed in *Salmonella*-infected mice on a C57BL/6 × 129 mixed

background (Fig EV5B and C). The vast majority of WT mice die around 5–7 dpi following a streptomycin pretreatment and 10^8 cfu *Salmonella* inoculation. A prolonged assessment of CD74$^+$ PCs after an infection by 10^7 *Salmonella* without streptomycin pretreatment suggested that a modest expansion of CD74$^+$ PCs persisted at least up to 9 d.p.i (Fig EV5E).

To investigate if other enteric pathogens may cause similar changes, we infected cefoperazone-pretreated C57BL/6 mice with

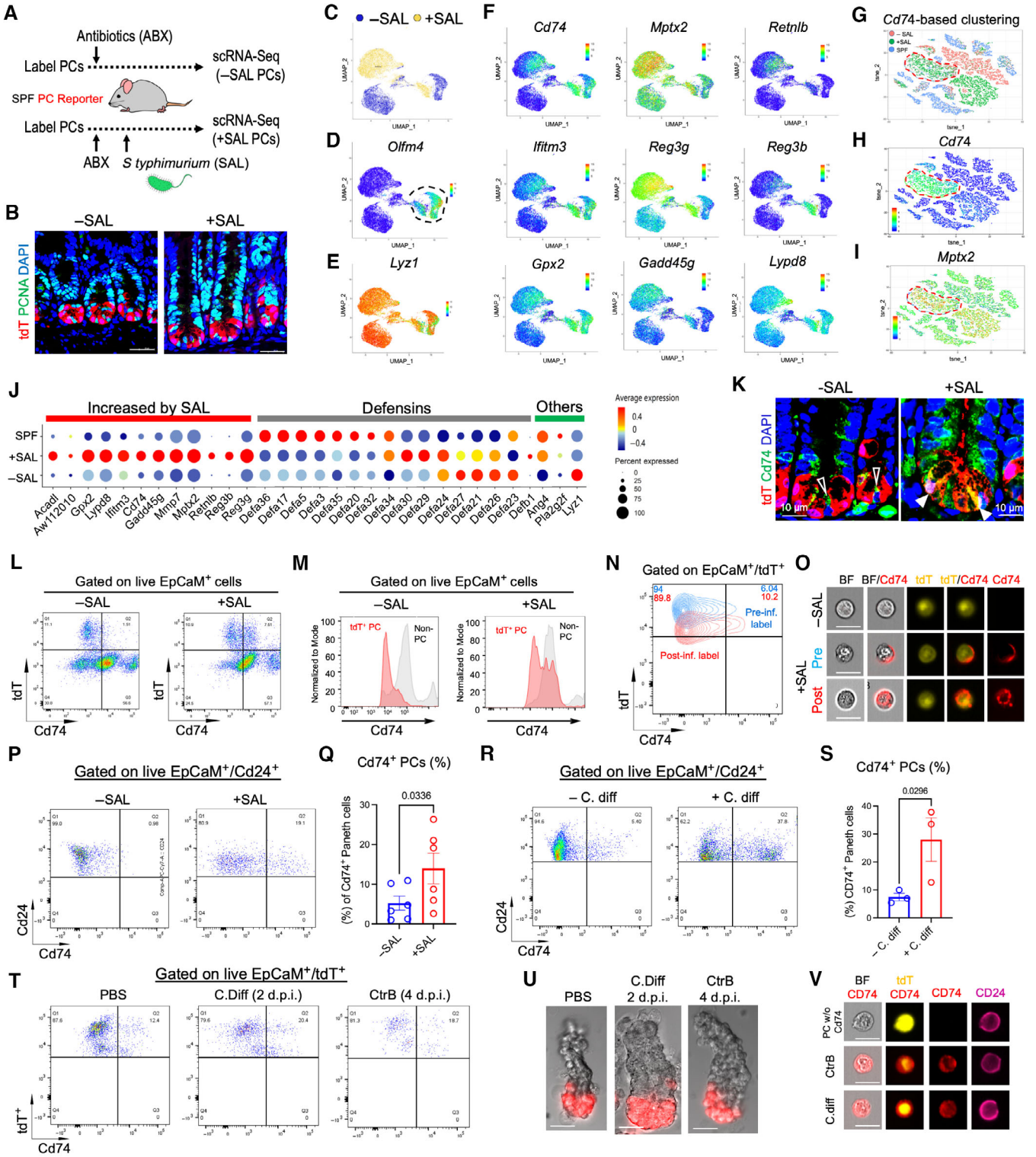

Figure 3.

Figure 3. Pathogen infection expands Cd74$^+$ Paneth cells.

A PC reporter mice were injected with tamoxifen to label PCs, and orally gavaged with 15 mg streptomycin dissolved in PBS. One day later, mice were divided into two groups: one group was gavaged with 10^8 CFU *Salmonella* (+SAL) and the other group was gavaged with sterile PBS (−SAL). All mice were sacrificed 4 days after inoculation. Ileal tdT$^+$ Paneth cells from −SAL and +SAL mice were FACS-sorted for scRNA-Seq analysis.

B Representative immunofluorescent analysis for tdT and PCNA in ilea of uninfected (−SAL) and *S. typhimurium*-infected (+SAL) reporter mice. Scale bars, 20 μm.

C UMAP analysis of −SAL (blue) and +SAL (yellow) ileal Paneth cells (total 16,530 cells).

D UMAP analysis of *Olfm4*-expressing progenitor PCs circled by dotted line.

E UMAP analysis of *Lyz1*-expressing PCs.

F UMAP analysis of 9 most highly elevated transcripts in +SAL PCs comparing to −SAL PCs.

G–I t-SNE analysis by *Cd74*-based clustering of SPF (blue), −SAL (red, with streptomycin treatment), and +SAL (green, with streptomycin and *Salmonella*) conditions. A cluster of Cd74^{high} PCs is circled by red dotted line in panel (H). This Cd74^{high} cluster also expresses high Mptx2, circled in panel (I).

J Dot plots comparing SPF versus −SAL versus +SAL PCs show the abundance of infection-induced signature genes, in addition to several known PC-enriched genes including Lyz1 and defensins.

K Representative immunofluorescent analysis of Cd74 (green) and tdT (red) in ilea of uninfected and *Salmonella*-infected PC reporter mice. Scale bars, 10 μm. Empty arrowheads point to Cd74$^+$ stem cells. Solid arrowheads point to Cd74$^+$ tdT$^+$ Paneth cells.

L FACS analysis of live crypt epithelial cells isolated from −SAL and +SAL PC reporter mice. Cells were gated on live EpCAM$^+$, then analyzed for tdT$^+$ and surface Cd74$^+$. Data represent five independent experiments performed on paired −SAL and +SAL mice analyzed on the same day.

M Histograms of PCs (red) and non-PC crypt epithelial cells (gray) show the change of normalized abundance of Cd74-expressing cells in −SAL and +SAL mice. *X*-axis represents Cd74 expression.

N PCs were labeled either before (blue) or after (red) *Salmonella* infection in paired littermates. Mice were sacrificed on the same day for FACS analysis. Cells were gated on live EpCAM$^+$/tdT$^+$ PCs and analyzed for Cd74 expression. Results represent two independent experiments.

O ImageStream of live tdT$^+$ PCs stained by Cd74 and tdT in −SAL and +SAL mice where PCs were labeled before (pre-) or after (post-) infection. Images represent > 200 cells of each condition. Scale bars, 5 μm.

P, Q FACS analysis of crypt epithelial cells from wild type C57BL/6 mice of −SAL and +SAL conditions. Cells were gated on live, EpCAM$^+$, Cd24$^+$ large cells (PCs), and analyzed for percentages of Cd74$^+$ PCs in −SAL and +SAL littermates (n = 5–6 mice each group). Data were analyzed by unpaired t-test from three independent experiments. Error bars represent SEM.

R, S FACS analysis of crypt epithelial cells from wild type C57BL/6 mice pretreated with cefoperazone, and infected (+C. diff) or not infected (−C. diff) with *C. difficile*. On 2 d.p.i, ileal epithelial cells were gated on gated on live, EpCAM$^+$, CD24 large (Paneth cells) cells and analyzed for percentage of Cd74$^+$ PCs of each condition (n = 3 mice each). Results were analyzed by paired t-test from two independent experiments. Error bars represent SEM.

T FACS analysis of tdT$^+$ PCs from reporter mice that were uninfected (PBS), infected with *C. difficile* 2 d.p.i, or infected with *Citrobacter* 4 d.p.i. Cells were gated on live, EpCAM$^+$, tdT$^+$ cells and analyzed for Cd74, which represent two independent experiments.

U Representative crypts isolated from uninfected (PBS), *Citrobacter*- or *C. difficile*-infected PC reporter mice that were imaged for direct tdT fluorescence under an epi-fluorescent microscope. Scale bars, 20 μm.

V ImageStream analysis for single Paneth cells stained with Cd74, Cd24, and tdT from uninfected (PBS), *Citrobacter*- or *C. difficile*-infected PC reporter mice. Results represent > 200 images for each condition. Scale bars, 5 μm.

Source data are available online for this figure.

Clostridioides difficile, a pathogenic bacterium associated with hospital acquired infection, severe colitis, and sometimes ileum involvement (McDonald *et al*, 2005; Chang *et al*, 2008; Reeves *et al*, 2011; Tsiouris *et al*, 2012; Lessa *et al*, 2015). Comparing to mice only treated with cefoperazone, *C. difficile* significantly increased percentage of CD74$^+$/CD24$^+$/EpCAM$^+$ PCs at 2 d.p.i. (Figs 3R and S, and EV5F). Similar results were obtained in *C. difficile*-infected PC reporter mice gated for tdT$^+$/CD74$^+$ (Fig 3T), and the effect was less in mice infected by *Citrobacter rodentium*, an epithelial adherent pathogenic bacterium similar to the human enteropathogenic *E. coli* (Luperchio *et al*, 2000; Luperchio & Schauer, 2001; Wiles *et al*, 2004). CD74$^+$ non-PCs increased by 1.86- and 1.23-fold by *C. difficile* and *C. rodentium*, respectively. Interestingly, even though these pathogens are known to cause primary inflammation in colon (Wiles *et al*, 2004), ileal crypts of infected mice were inflamed (Figs 3U and EV5G). Image Stream analysis verified the robust CD74 expression in PCs from *C. difficile* or *C. rodentium* infected mice (Fig 3V).

Activated CD74$^+$ PCs secrete immune regulatory molecules

fGSEA comparison of the transcriptome of CD74$^+$ PCs versus CD74$^-$ PCs (reads of CD74 = 0) from +SAL mice suggested that CD74$^+$ PCs have elevated transcriptomes for oxidative phosphorylation (OXPHOS), degranulation, autophagy, ROS signaling, IFNα, and innate response to infection ($P < 0.001$, Fig 4A). CD74$^+$ PCs contain more transcripts for receptors of IFNg, IL17, IL22, IL1, as well as cytokines and growth factors such as MIF, Wnt3, Dll, EGF (Fig 4B). To screen for secreted proteins from CD74$^+$ PCs, reporter mice (n = 3 for each sample) were infected by *Salmonella*, CD74$^+$/tdT$^+$ PCs were sorted on 4 d.p.i., pooled, and resuspended in base culture medium. Using a proteome-based antibody array, the secretome were probed for a total of 111 mouse cytokine, chemokine, and growth factor. Protein targets enriched in CD74$^+$ PC secretome against blank medium were identified (Figs 4C and EV5H and I), with the top 20 ranked by abundance (Fig 4D). Reg3G (a C-type lectin) and Pentraxin 3 were most abundant, while Mmp2 (a matrix metallopeptidase similar to Mmp7), Ang1 and Ang5 (homologous to Ang4) are antimicrobial proteins, and DKK, DLK-1, and LIF are regulators of stem cells (Ceder *et al*, 2008; Zhu *et al*, 2009; Onishi & Zandstra, 2015). We also noted the production of interferon ligand (IL-28) (Witte *et al*, 2010), myeloperoxidase (Klinke *et al*, 2011), and chemokines: CCL19 (Comerford *et al*, 2013), CCL17 (Feng *et al*, 2022), and CCL6 (Coelho *et al*, 2007), all of which are potent chemotactic molecules attracting immune cells to the site of inflammation.

Paneth cells secrete various AMPs in response to inflammatory stimulations (Rumio *et al*, 2004; Farin *et al*, 2014; Stockinger *et al*, 2014; Yokoi *et al*, 2019). When compared to CD74-negative PCs, the transcriptome of CD74$^+$ PCs is enriched with 114

degranulation factors (Fig EV5J) related to the structure and function of secretory granules, suggesting that CD74$^+$ PCs may be primed for secretion. Infection induces innate immune cells, such as neutrophils, to release intracellular ROS via secretory granules (Karlsson & Dahlgren, 2002; VanderVen *et al*, 2009; Nordenfelt & Tapper, 2011; Nguyen *et al*, 2017), and *S. typhimurium* induces host

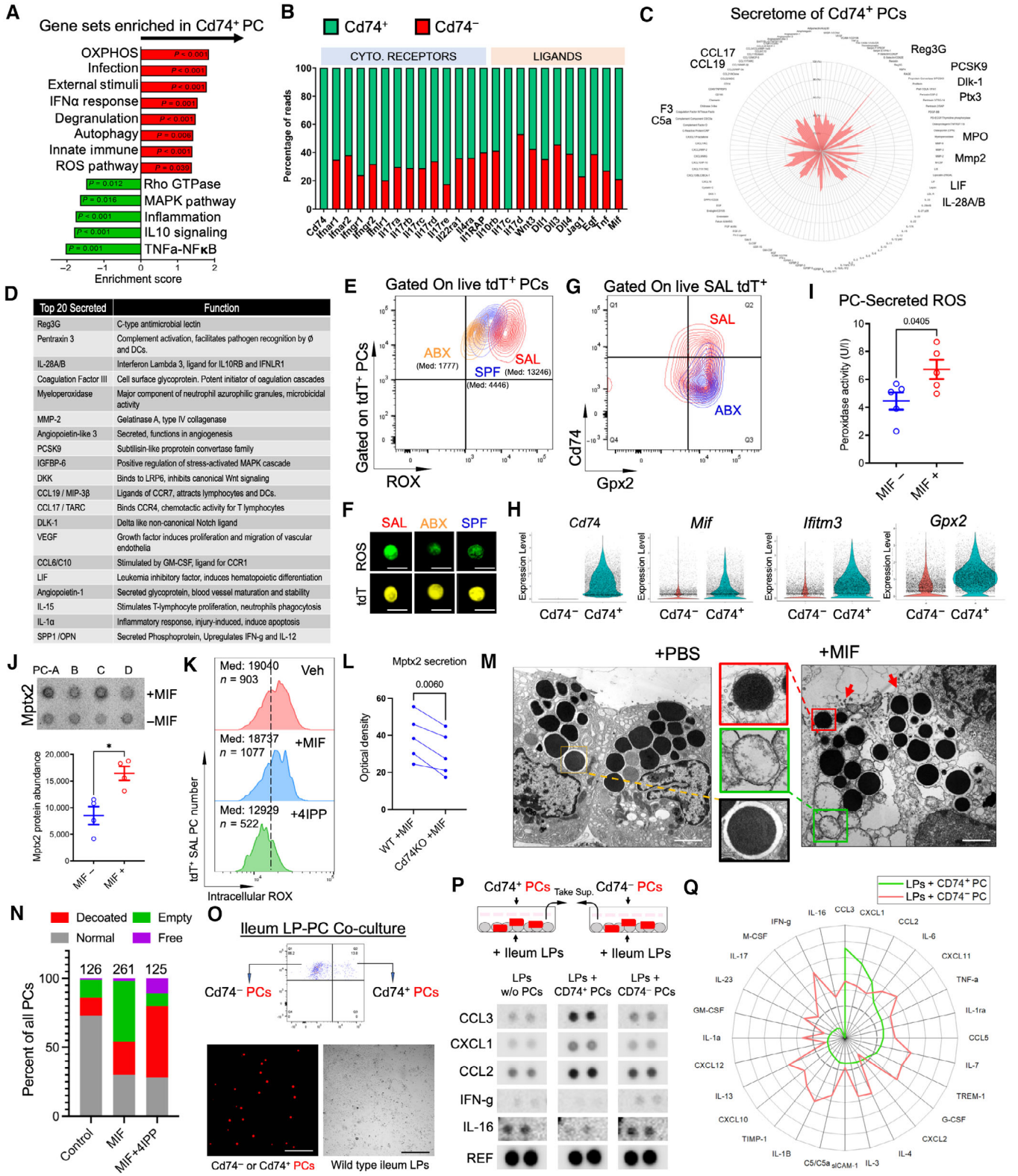

Figure 4.

Figure 4. Infection activated Cd74$^+$ Paneth cells to secrete ROS and inflammatory molecules.

A fGSEA analysis comparing Cd74$^+$ and Cd74$^-$ PC transcriptomes shows that the top enriched gene sets are OXPHOS, infection, IFN response, degranulation, autophagy, and ROS pathway ($P < 0.001$).

B Proportion of total transcripts of a list of cytokine receptors, cytokines, and growth factors in Cd74$^+$ (red) and Cd74$^-$ (green) PCs in +SAL mice.

C Live tdT$^+$/Cd74$^+$ PCs were FACS sorted from *Salmonella*-infected PC reporter mice, pooled, and seeded in base culture medium. After 16 h, supernatants from the PC culture were collected for a proteome-based secretome analysis on a 111-cytokine array (duplicate dots per cytokine). Blank medium was used for baseline for each cytokine. The average densitometry values "Cd74$^+$ PCs minus blank medium" for individual cytokines were transformed by natural Log and plotted in an alphabetical order. Targets with high peak are labeled in red.

D The top 20 secreted proteins, based on absolute abundances, are listed in order.

E FACS analysis for intracellular cell ROX on PCs sorted from SPF, −SAL (ABX), and +SAL mice, which represent three independent experiments.

F ImageStream of cell ROX-stained single PCs isolated from SPF, −SAL (ABX), and +SAL mice. Scale bars, 5 μm.

G FACS analysis for Cd74 and Gpx2 in cells gated on live tdT$^+$ PCs of +SAL mice and −SAL (ABX) mice.

H Violin plots made from scRNA results show the transcript abundances of *Mif*, *Ifitm3*, and *Gpx2* in *Cd74*$^+$ and *Cd74*$^-$ PCs.

I 6,000 FACS-sorted tdT$^+$ PCs from +SAL mouse ilea were treated *ex vivo* with either PBS or recombinant MIF for 30 min. Peroxidase activity was measured from 10 μl of supernatants. Results were analyzed by unpaired *t*-test from five mice in two independent experiments. Error bars represent SEM.

J 6,000 FACS-sorted tdT$^+$ PCs from +SAL mouse ilea were treated *ex vivo* with either PBS or recombinant MIF for 30 min. Mptx2 proteins were measured from supernatants by dot blotting assay. Densitometry values were analyzed by unpaired *t*-test from five mice in two independent experiments. Error bars represent SEM.

K Intracellular ROX were measured by FACS from sorted single tdT$^+$ PCs treated *ex vivo* by PBS ($n = 903$ cells), MIF ($n = 1{,}077$ cells), and by MIF plus 4-IPP ($n = 522$ cells). Data represent two independent experiments.

L Sorted EpCAM$^+$/Cd24$^+$ Paneth cells from paired WT and Cd74$^{-/-}$ mice ($n = 5$ for each genotype) were treated *ex vivo* by MIF. Mptx2 was quantified from supernatants by dot blots analysis. Paired *t*-test was used for statistical comparison.

M TEM micrographs of sorted tdT$^+$ PCs that were treated by PBS or by MIF *ex vivo*. Arrows point to degranulated dense core particle. Scale bars, 1 μm.

N Based on the granule morphologies characterized as "normal," "de-coated," "empty," and "free" (outside of the cells), percentages of each morphology were determined from a total of 126, 216, and 125 granules from PCs treated by PBS, MIF-, or MIF/4-IPP, respectively.

O Diagram shows that live Cd74$^-$ and Cd74$^+$ PCs were flow-sorted from infected reporter mice and pooled. Same number of Cd74$^-$ or Cd74$^+$ PCs (4,377) were seeded for co-culture with wild type ileal lamina propria cells. After 16-h co-culture, representative images of the co-culture were taken under epi-fluorescent and brightfield microscope. Scale bars, 200 μm.

P Supernatants were taken from PC/LP co-culture and determined for cytokine production using an antibody-based cytokine array. Supernatants from lamina propria cells alone (without PCs) were blotted on paired arrays to serve as baseline. Representative cytokines that were changed in Cd74$^+$ PC/LP co-culture were shown.

Q For each cytokine, average densitometry values of technical duplicates from Cd74$^-$ PC/LP or Cd74$^+$ PC/LP co-cultures were normalized against LP monoculture. The ratios were log-transformed and presented on radar plots (green: Cd74$^+$ PC/LP co-culture; red: Cd74$^-$ PC/LP co-culture). Results represent two independent experiments.

Source data are available online for this figure.

cell ROS production (Winter *et al*, 2010). No study has tested ROS production by PCs to our knowledge. Flow cytometry quantification of intracellular ROS in live PCs from SPF, −SAL, and +SAL mice revealed that PCs in infected mice contained the highest ROS, 3- and 7.5-fold more than SPF and −SAL PCs, respectively (Fig 4E and F). High Gpx2, an intracellular ROS scavenger (Chu *et al*, 1993; Schafer & Buettner, 2001; Moine *et al*, 2018), was found in 80.4% of Cd74$^+$ PCs and 70.9% of Cd74$^-$ PCs (Fig 4G), in agreement with its transcriptional abundance in Cd74$^+$ PCs (Fig 4H).

MIF is an inflammatory cytokine that activates CD74 (Naujokas *et al*, 1993; Leng *et al*, 2003; Shi *et al*, 2006), and its transcript (*Mif*) was enriched by CD74$^+$ PCs (Fig 4H). Treating +SAL PCs with recombinant MIF *ex vivo* elicited a significant secretion of ROS into the medium (Fig 4I). MIF treatment also elicited the secretion of Mptx2 (Fig 4J), the pentraxin enriched in CD74$^+$ PCs (Fig 3F, H and I). Treating +SAL PCs with MIF did not further increase intracellular ROS, likely due to the enhanced ROS release. However, addition of 4-iodo-6-phenylpyrimidine (4-IPP), an inhibitor of MIF/CD74 (Winner *et al*, 2008) reduced intracellular ROS (Fig 4K). In addition, PCs flow-sorted from unchallenged Cd74$^{-/-}$ mice produced less Mptx2 proteins upon MIF stimulation *ex vivo*, compared to PCs sorted from wild type mice (Fig 4L), suggesting that loss of CD74 decreased MIF-stimulated Mptx2 secretion. Interestingly, for PCs sorted from *Salmonella*-infected mice, neither 4-IPP nor a CD74 neutralizing antibody (Clone LN-2) (Schwartz *et al*, 2009) blocked Mptx2 secretion after MIF stimulation (Fig EV5J), suggesting that infection-induced Mptx2 was not exclusively controlled by CD74. Transmission EM analysis showed that MIF treatment, within 20 min, robustly increased degranulating vesicles with an uncoated morphology reflecting an exuberated granule release (Figs 4M and N, and EV5K). This enhanced degranulation was consistent with the enriched degranulation gene network in CD74$^+$ PCs, based on our scRNA data (Fig EV5L). These results suggest that infection and inflammatory cytokines (e.g., MIF) may activate CD74$^+$ PCs for the production of ROS and mucosal pentraxin Mptx2.

To test if CD74$^+$ PCs interact with resident lamina propria (LP) cells, we co-cultured wild type mouse ileal LP cells with equivalent numbers of live CD74$^+$ or CD74$^-$ PCs sorted and pooled from *Salmonella*-infected PC reporter mice ($n = 3$ for each sample, Fig 4O). Supernatants collected from a 16-h co-culture were probed by a cytokine array. Compared to LP/CD74$^-$ PC co-culture, LP/Cd74$^+$ PC co-culture produced more CCL2 (Reinecker *et al*, 1995; Ashida *et al*, 2001), CCL3 (Maurer & von Stebut, 2004), and CXCL1 (Mitsuyama *et al*, 2006; Alzoghaibi *et al*, 2008; Li *et al*, 2015), chemokines that recruit inflammatory cells to site of infection (Fig 4P and Q). These chemokines are known to be produced by various LP cell types, including neutrophils and mesenchymal cells (Riedel & Kaufmann, 1997; Blidberg *et al*, 2012; Jung *et al*, 2013; Palomino & Marti, 2015; Tecchio & Cassatella, 2016; Stzepourginski *et al*, 2017). Less IL-16, IFNγ, M-CSF, and IL-17 were produced by LP/CD74$^+$ co-culture (Figs 4P and Q, and EV5L and M), suggesting that CD74$^+$ PCs interact with LP cells differently from Cd74$^-$ PCs.

CD74$^+$ PCs expand in human IBD and correlate with disease progression in mouse colitis models

To determine if *CD74*$^+$ PCs also exist in human and expand in inflammatory diseases, we performed RNA base-scope analysis

using specific probes for *CD74* (in blue) and *LYZ* (in red). 12.9% of PCs in non-IBD intestinal tissues were $CD74^+$ ($n = 12$), while 59.2, 40.4, and 46.2% of PCs in UC ($n = 6$), CD ($n = 4$), and GvHD ($n = 6$) showed $CD74^+$, respectively (Fig 5A, Appendix Fig S1A). Glands with obvious inflammation contained over 90% $CD74^+LYZ^+$ PCs. The abundances of *CD74* transcripts per PC were also increased by 763, 756, and 668% for UC, CD, and GvHD compared to non-IBD tissues (0.62 transcripts per PC) (Fig 5B). We evaluated CD74 protein expression in HD5 or LYZ-positive PCs in IBD involved tissues ($n = 21$ CD and 15 UC). $CD74^+HD5^+$ or LYZ^+ PCs were observed in CD ileum (Fig 5C and D), and UC metaplastic lesions in descending colon or rectum (Fig 5E, Appendix Fig S1B), albeit the frequencies were low. Judged from fluorescent intensities, $CD74^+$ PCs contained lower CD74 abundance than adjacent $CD74^+$ immune cells. The lower frequency of CD74 protein-expressing PCs compared to *CD74* transcripts suggest that these cells may transiently correlate with active phase of inflammation.

We then investigated the developmental dynamics of $CD74^+$ PCs in $TNF^{\Delta ARE/+}$ mice, a model of chronic ileitis triggered by aberrant inflammatory cytokine (Kontoyiannis *et al*, 1999). In 4-week old $TNF^{\Delta ARE/+}$ mice, $Cd74^+$ PCs were barely detected in the ileum (Fig 5F); however, they became evident at 8 weeks, the onset of inflammation (Fig 5G). The frequency of $Cd74^+$ PCs increased by 133 and 145% at 10 and 17 weeks, respectively (Fig 5H and I). These $Cd74^+$ PCs tend to appear in inflamed crypts. Although there was a temporal decline in the number of lysozyme-expressing PCs as the ileitis progressed, the number of $Cd74^+$ PCs per crypt increased (Fig 5J). These results suggested that an increased proportion of $Cd74^+$ PCs was correlated with ileitis progression.

We further investigated the dynamic of $Cd74^+$ PCs in GvHD mouse models, where the inflammation is triggered by allogeneic T-cell transplantation. At 8, 22, and 38 days following disease induction, $Cd74^+$ PCs were readily detected in sites of active inflammation (Fig 5K, Appendix Fig S1C). Evaluating mouse cohorts with intragroup disease variations indicated that the frequency of $Cd74^+$ PC events was positively correlated with the degree of pathology ($r = 0.74$, Fig 5L). $TNF^{\Delta ARE/+}$ and GvHD models were established on mice of different genetic background. These results showed that inflammation triggered by auto and allogeneic immune responses can also trigger the expansion of $Cd74^+$ PCs.

Paneth cell specific MyD88-deficient mice had reduced $Cd74^+$ PCs and inflammation

We next sought to investigate if PCs' microbial sensing capability regulate their composition. Being the downstream adaptor for TLR signaling pathways, *MyD88* transcripts were detected in 4.8% of PCs in SPF mice, and were distributed across progenitor and mature duodenal and ileal PC populations (Fig 6A, Appendix Fig S2A). Mice treated with streptomycin had 2.9% of $MyD88^+$ PCs, while *Salmonella* infection increased $MyD88^+$ PCs to 5.1% (Appendix Fig S2A). We then developed PC-specific *MyD88* knockout mice ($MyD88^{\Delta PC}$) using $Lyz1^{3'UTR\text{-}CreER}$ as a driver. Deletion of floxed *MyD88* in FACS-sorted PCs was validated by genomic PCR (Fig 6B). $MyD88^{\Delta PC}$ mice did not show overall abnormality in PC number in homeostasis. Upon *Salmonella* infection, $MyD88^{\Delta PC}$ ileal crypts became elongated, and *MyD88*-deficient PCs showed a robust upward localization in upper crypt or villus regions (Fig 6C and D), a phenotype reminiscent of defective EphB/ephrinB signaling (Batlle *et al*, 2002). This observation was also noted in isolated $MyD88^{\Delta PC}$ crypts (Fig 6E). Comparing to WT mouse PCs, these abnormally localized *MyD88*-deficient PCs had reduced *Lyz1* or *Ang4* (Fig 6F and G), and a reduction in Mptx2 (Fig 6H and I). A significant reduction of fecal Mptx2 was also found in $MyD88^{\Delta PC}$ mice (Fig 6J). FACS analysis showed a reduction of $Cd74^+$ PCs in infected $MyD88^{\Delta PC}$ mouse ileum comparing to WT littermates (Fig 6K and L, Appendix Fig S2B). Intracellular Cd74 staining after permeabilization showed a reduction in total number of $Cd74^+$ cells (Appendix Fig S2C) as well as total Cd74 abundance (based on fluorescent intensity) in the remaining $Cd74^+$ PCs in $MyD88^{\Delta PC}$ PCs compared to WT PCs (Appendix Fig S2D). These results suggest that deleting *MyD88* in PCs affected their composition and secretion of Mptx2.

We then examined if *MyD88*-deficient PCs mediate different cross talks with resident lamina propria cells. We co-cultured WT ileal LPs with PCs isolated from *Salmonella*-infected WT or $MyD88^{\Delta PC}$ littermates (Fig 6M). LP+WT PC co-culture elicited TIMP-1, M-CSF, CCL2, and CXCL1, which were reduced in LP+MyD88-deficient PC co-culture (Fig 6N and O, Appendix Fig S2E). CCL2 and CXCL1 are two highly chemoattractant for neutrophils and monocytes (Bozic *et al*, 1995; Gu *et al*, 1999), and both were elicited by LP and $Cd74^+$ PC co-cultures (Fig 4P and Q). In contrast, LP+MyD88-deficient PC co-culture produced more IL-1a and IL-1b (Fig 6N and O, Appendix Fig S2E). These results suggested that PCs lacking MyD88 had altered cross talks with resident LPs.

Salmonella-infected $MyD88^{\Delta PC}$ mice revealed an overall reduced gut inflammation and an ameliorated systemic disease activity, comparing to WT littermates, reflected by body weight (Fig 6P), ileocolic inflammation (Fig 6Q and R), bacterial dissemination in spleen (Fig 6S, Appendix Fig S2F). Infected $MyD88^{\Delta PC}$ mice did exhibit similarly abnormal cecum (Appendix Fig S2G), intestinal permeability (Appendix Fig S2H), and *Salmonella* CFUs in mesenteric lymph nodes (Appendix Fig S2I), suggesting that the reduced morbidity in $MyD88^{\Delta PC}$ mice was not due to a reduced *Salmonella* virulence or infection efficacy.

We then investigated the LP immune cell profile in infected $MyD88^{\Delta PC}$ and WT littermates. FACS analysis revealed a significant reduction in $Ly6G^+$ neutrophil (Fig 6T and V), and moderate reductions in $CD4^-/F4/80^+$ macrophage (Fig 6U and W) and $CX3CR1^+/CD11c^+$ dendritic cells (Appendix Fig S2J) in $MyD88^{\Delta PC}$ mouse ileum. No change was found in $CD103^+/CD11c^+$ dendritic cells (Appendix Fig S2K), T cells (Appendix Fig S2L), or total $MHCII^+$ cells (Appendix Fig S2M). $CX3CR1^+/CD11c^+$ and $CD103^+/CD11c^+$ dendritic cells have been shown to mediate systemic dissemination of *Salmonella* in mice (Diehl *et al*, 2013). Immunostaining confirmed the significant reduction in neutrophil recruitment in $MyD88^{\Delta PC}$ ileum after infection (Fig 6X–Z). Macrophages and T-cell populations were modestly reduced (Appendix Fig S2N) or unchanged (Appendix Fig S2O). These data suggest that lacking MyD88 in PCs affected immune cell recruitment and inflammatory progression.

Abrogating Mptx2 reduces complement activation and inflammation

Compared to luminal abundances of lysozyme or defensins α-1, the temporal kinetics of luminal Mptx2 was different (Fig 1G). In SPF

mice, unlike *Lyz1*, PCs with high *Mptx2* represent a smaller population enriched in ileum (Fig EV2H). Abundance of *Mptx2* was elevated in ileal PCs by microbiota transfer in GF mice (Fig 2G and J). Immunostaining for Mptx2 revealed that mouse ileum had more Mptx2 PCs than duodenum (Fig 7A and B). *Salmonella* infection promoted Mptx2 in ileal PCs (Fig 7C and D). Comparing to uninfected mice, Mptx2 in infected mouse PCs became more granulated (Fig 7C), with increasing number of extracellular Mptx2-containing

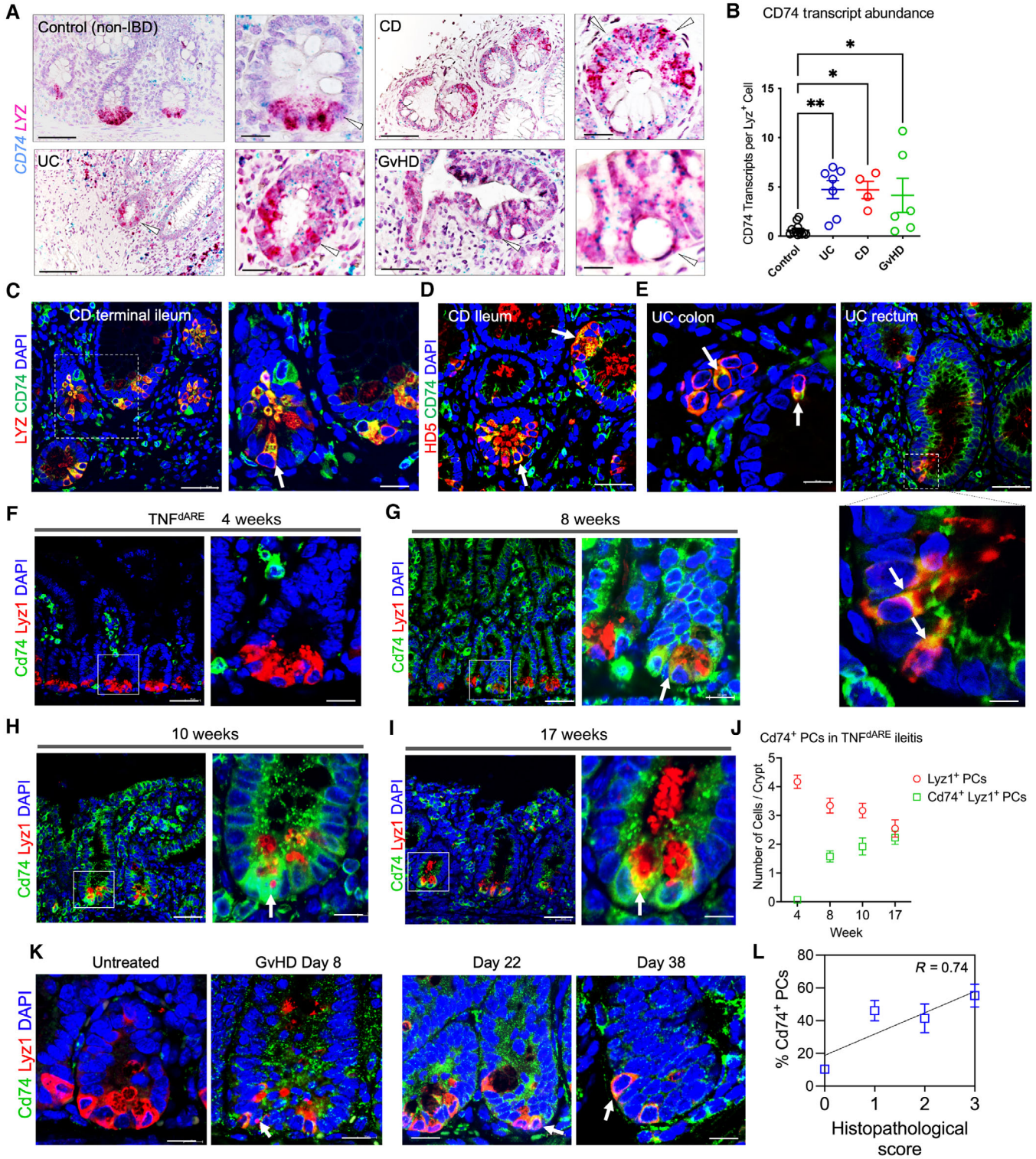

Figure 5.

Figure 5. Abundance of CD74$^+$ Paneth cells correlate with inflammatory disease development.

A Using probes specific for human *CD74* (in blue) and *LYZ* (in red), dual RNA base-scope analyses were performed on CD, UC, GvHD, and non-IBD patient tissues. Representative images were shown, with arrows pointing to *CD74*$^+$/*LYZ*$^+$ glandular cells. Scale bars, 50 μm; and 20 μm in high magnifications.

B Three to six independent fields, where Paneth cells were found, were imaged for each patient sample of UC ($n = 6$), CD ($n = 4$), GvHD ($n = 6$), and non-IBD ($n = 12$). CD74 transcript numbers per Paneth cells were counted, and the averages were plotted for each individual patient. Data represent mean ± SEM. *$P < 0.05$; **$P < 0.01$.

C CD patient ilea ($n = 21$) were immunostained for CD74 and lysozyme. Arrows point to double-positive cells.

D CD patient ilea ($n = 21$) were immunostained for HD5 and CD74. Arrows point to double-positive cells.

E UC patient ($n = 15$) descending colon (left) and rectum (right) were stained for HD5 and CD74. Arrows point to double-positive cells.

F–I Immunofluorescent staining for Cd74 and lysozyme in TNF^{dARE} mouse ilea of 4 weeks (F), 8 weeks (G), 10 weeks (H), and 17 weeks (I) of age. Scale bars, 50 μm; and 20 μm in high magnifications. Arrows point to Cd74$^+$ Paneth cells.

J Numbers of lysozyme$^+$ Paneth cells (red) and lysozyme$^+$/Cd74$^+$ cells (green) per crypt were counted from 22 to 41 crypts from five independent mice of each time point. Data are plotted as mean and SEM for each time point.

K To induce GvHD, irradiated BALB/c mice were transplanted with donor B6 T-cell-depleted BM cells mixed with CD4$^+$ T cells. Whole small intestines were dissected after 8, 22, and 38 days of disease induction. Representative immunostaining images of Cd74 and lysozyme were shown for untreated and diseased tissues at different time points. $N = 5$–6 mice for each time point. Scale bars, 20 μm.

L From a cohort of 10 mice at 22 and 38 days after T-cell transplantation, percentage of Cd74$^+$ Paneth cells were determined by immunostaining from different tissue fields characterized as no inflammation (0), low (1), moderate (2) and severe (3) inflammation. The correlation coefficient (r) analysis was performed between Cd74$^+$ PC percentage and inflammatory severity and was determined as 0.74. Data represent mean ± SEM.

Scale bars in panel (C–E), 50 μm; and 20 μm in high magnifications.
Source data are available online for this figure.

granules detected in proximity to *Salmonella* (Fig 7E and F). The luminal Mptx2 granule was also reduced in infected *MyD88*$^{\Delta PC}$ ileal lumen (Appendix Fig S2P). Further, we verified a significantly increased fecal Mptx2 in *Salmonella*-infected mice (Fig 7G and H). These results suggested that infection stimulates Mptx2 abundance and secretion by PCs.

Pentraxin family proteins are innate immune molecules implicated in promoting inflammatory responses via complement activation (Ma & Garred, 2018). To investigate the *in vivo* role of this PC-specific mucosal pentraxin, we developed *Mptx2* knockout mice by CRISPR-CAS9 genome editing. One founder was identified to have a 19-bp deletion in exon 2 of *Mptx2* resulting in a frame-shift and premature stop codon. Western blots on ileum lysates confirmed the successful Mptx2 deletion in *Mptx2Δ19/Δ19* knockouts (Fig 7I). Immunostaining verified a diminished Mptx2 immunoreactivity in knockout mouse ileal PCs (Fig 7J).

Mptx2$^{-/-}$ mice are healthy and fertile in homeostasis. When challenged by *Salmonella* infection, *Mptx2*$^{-/-}$ mice showed modestly improved body weight (Appendix Fig S3A), reduced ileocolonic inflammation (Fig 7K–M, Appendix Fig S3B), and reduced neutrophils in ileum and colons (Fig 7N–P, Appendix Fig S3C), compared to WT littermates. Interestingly, *Mptx2*$^{-/-}$ mice showed significantly reduced *Salmonella* dissemination to the spleens although no difference was found in MLNs and livers (Fig 7Q and R, Appendix Fig S3D), an observation surprisingly similar to *MyD88*$^{\Delta PC}$ mice (Fig 6S). Infection induced complement activation correlates to systemic inflammation, our examination of the classical, alternative, and lectin complement pathways revealed significantly reduced ileal and serum MASP1 in *Mptx2*$^{-/-}$ mice (Fig 7S–V, Appendix Fig S3E). FACS analysis of infected *Mptx2*$^{-/-}$ and WT mice did not detect significantly changed frequency of CD74$^+$ PCs (Appendix Fig S3F) or changed lysozyme expression (Appendix Fig S3G). These results suggest that Mptx2 secreted by PCs during a typical infection activates lectin complement pathway propagating the systemic inflammatory disease state. Taken together, we propose that commensal and pathogenic bacteria modulate PC population towards an immune-regulatory feature, which is integral to regulating innate immune response and disease progression.

Discussion

Paneth cells contribute to the first line of intestinal innate immune system (Patel & McCormick, 2014) by secreting AMPs (Kamioka *et al*, 2022), shaping the microbiota, regulating mucin-producing goblet cells, and engaging in epithelial plasticity (Salzman *et al*, 2003b, 2010; Bevins & Salzman, 2011; VanDussen *et al*, 2014; Liu *et al*, 2016, 2018; Yu *et al*, 2018, 2020). Whether and how commensal and pathogenic microbes affect PC transcriptomic heterogeneity and function were not incompletely resolved on single cell level. Using the newly developed inducible PC reporter, we produced an in-depth single cell transcriptomic map on highly enriched PC populations from SPF, GF, and infected mice. These approaches allowed uncovering low-copy transcripts and increasing confidence in genes such as *MyD88* and various cytokine receptors, expressed only by small fractions of PCs. In addition to deepening the insight on transcriptomic differences in regional PCs (Darmoul & Ouellette, 1996; Haber *et al*, 2017), our data uncovered a microbe-regulated, infection, and inflammation-activated PC subset carrying transcriptomic signatures different from steady-state mature or progenitor PCs. The gnotobiotic experiments confirmed that gut microbiota is not required for PC development. In addition, our data concluded that a total gut commensal microbiota or specific bacterial species modify PC transcriptome towards specialized functions, such as making more Reg3g, Mptx2, Mmp7, etc. Pathogenic infection expanded and activated a group of PCs that are prone to degranulation and production of pro-inflammatory proteins and ROS. These PCs can be identified by their expression of Cd74. The events of these cells correlate positively with inflammatory diseases in human and mouse enteritis models.

Mice with PC-specific deletion of *MyD88* had reduced Cd74$^+$ PCs. Our scRNA results suggest that *MyD88* is expressed in about 5% of PCs. Surprisingly, disrupting *MyD88* in PCs dampened inflammatory response to infection. Earlier study overexpressing *MyD88* in mouse PCs showed that PC-intrinsic MyD88 signaling limited bacterial penetration of host tissues (Vaishnava *et al*, 2008). We observed a mitigated disease severity and a reduced bacterial dissemination to spleen in *MyD88*$^{\Delta PC}$ mice. *MyD88*$^{\Delta PC}$ mice do not have differences

from WT mice in terms of cecum abnormality or local bacterial penetration (i.e., CFUs in MLN), suggesting that the ameliorated systemic infection was not due to reduced bacterial virulence or invasiveness. *Salmonella*-induced gut inflammation conferred colonization advantages to the pathogen that makes use of the increased production of ROS for respiration (Winter *et al*, 2010).

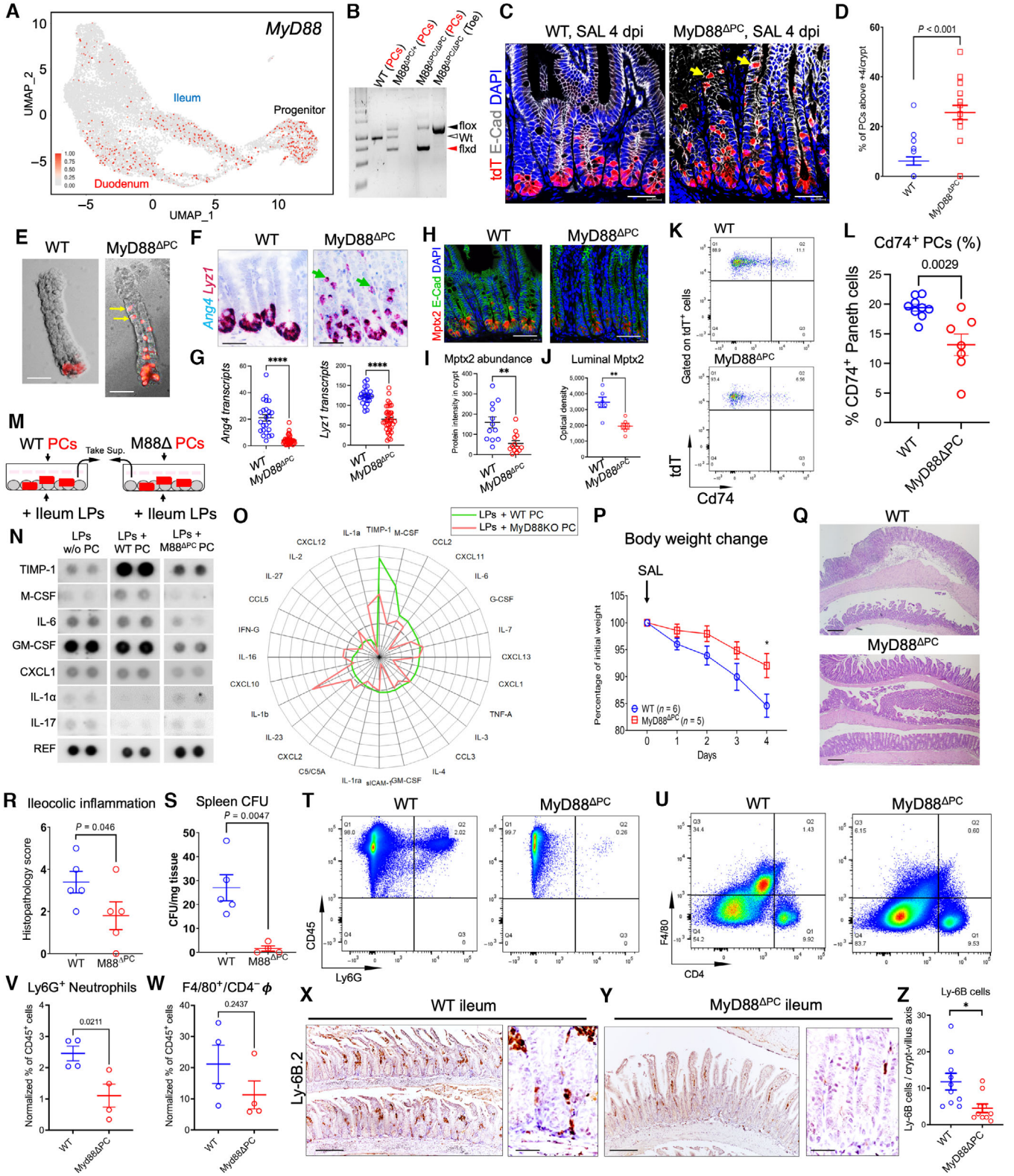

Figure 6.

Figure 6. Abolishing *MyD88* in Paneth cells affect PC function and systemic inflammation.

A Seurat UMAP analysis shows MyD88-expressing PCs in SPF mouse duodenum and ileum.

B Genomic PCR was done on DNA extracted from tdT$^+$ PCs flow sorted from WT (lane 1), heterozygous (lane 2), and *MyD88$^{Fl/Fl}$;Lyz1$^{3'UTR\text{-}CreER}$;R26R-tdT* (*MyD88$^{\Delta PC}$*) mice (lane 3). Primes specifically for amplifying floxed *MyD88* (pointed by red arrowhead) showed effective recombination (deletion). Toe DNA from *MyD88$^{\Delta PC}$* mice serve as negative control (lane 4).

C Representative immunostaining analysis for tdT (red) and E-Cad (white) in *WT* and *MyD88$^{\Delta PC}$* mouse ileum at 4 d.p.i. of *Salmonella* infection. Images represent 15–20 independent experiments. Arrows point to abnormal Paneth cells that migrated to villus. Scale bars, 50 μm.

D Number of tdT$^+$ cells above +4 position per crypt was counted and compared by unpaired *t*-test from 22 to 25 crypts of WT and MyD88$^{\Delta PC}$ mice ($n = 3$ for each genotype) infected with *Salmonella*.

E Representative images were taken under brightfield and epi-fluorescent microscope for crypts freshly isolated 4 d.p.i from WT and MyD88$^{\Delta PC}$ mice infected with *Salmonella*. Results represent at least five independent experiments. Arrows point to abnormal Paneth cells that migrated to villus. Scale bars, 50 μm.

F, G Dual RNA base-scope analysis was performed for *Ang4* (blue) and *Lyz1* (red) on WT and MyD88$^{\Delta PC}$ mouse ileal Paneth cells 4 d.p.i of *Salmonella* infection. Number of transcripts per crypts for *Ang4* (left) and *Lyz1* (right) were quantified by Image J from 20 to 25 crypts of WT or MyD88$^{\Delta PC}$ mice ($n = 3$ for each genotype), and compared in panel (G) with an unpaired *t*-test. Scale bars, 50 μm.

H, I Representative immunofluorescent staining for Mptx2 (red) and E-Cad (green) in WT and MyD88$^{\Delta PC}$ mice 4 d.p.i of *Salmonella* infection ($n = 3$ for each genotype). Average crypt Mptx2 protein abundances from 12 independent fields were compared by unpaired *t*-test in panel (I). Scale bars, 50 μm.

J Fecal Mptx2 protein abundances were determined by dot blots. Densitometry values for individual WT and MyD88$^{\Delta PC}$ biological replicates ($n = 5$) were compared by unpaired *t*-test.

K, L FACS analysis of tdT$^+$/Cd74$^+$ PCs in WT and MyD88$^{\Delta PC}$ mouse ilea 4 d.p.i of *Salmonella* infection. Percentages of Cd74$^+$ PCs of total PCs were compared by unpaired *t*-test from WT and MyD88$^{\Delta PC}$ biological replicates in three independent experiments.

M, N Paneth cells were sorted from WT versus MyD88$^{\Delta PC}$ mice ($n = 3$ each genotype) at 4 d.p.i. by *Salmonella* and pooled. 5,000 PCs of each genotype were seeded for co-culture with wild type lamina propria cells. After 16-h, antibody-based cytokine arrays were used to determine cytokine production from the co-cultures and from lamina propria cell alone (w/o PC). Representative cytokines changed in MyD88$^{\Delta PC}$ PC/LP co-culture are shown.

O For each cytokine, averaged densitometry values of technical duplicates from WT-PC/LP co-culture or MyD88$^{\Delta PC}$ PC/LP co-cultures were normalized against LP monoculture. The resulting ratios were log-transformed and presented on radar plots (green: WT-PC/LP co-culture; red: MyD88$^{\Delta PC}$ PC/LP co-culture). Results represent two independent experiments.

P Body weight changes of *WT* and *MyD88$^{\Delta PC}$* mice ($n = 5$ biological replicates for each genotype) after *Salmonella* infection.

Q, R Representative histology of infected WT and MyD88$^{\Delta PC}$ mouse ilea. Ileocolic inflammation was scored from ileum and colon of each mouse based on epithelial damage and immune cell infiltration detailed in Method ($n = 5$ mice for each genotype). Scale bars, 200 μm.

S Spleen *Salmonella* CFU was determined for each WT and MyD88$^{\Delta PC}$ mouse 4 d.p.i. Data were plotted as per mg of spleen tissue from five mice of each genotype.

T FACS analysis of Ly6G and CD45 cells in *Salmonella*-infected WT and MyD88$^{\Delta PC}$ mouse ileal lamina propria. LPLs were stained and viable cells were analyzed.

U FACS analysis of CD4 and F4/80 cells in *Salmonella*-infected WT and MyD88$^{\Delta PC}$ mouse ileal lamina propria. LPLs were stained and viable cells were gated on CD45$^+$ and analyzed for F4/80 (macrophage marker) and CD4 (murine macrophages are CD4$^-$).

V, W Unpaired *t*-test comparison of the percentages of viable CD45$^+$/Ly6G$^+$ neutrophils, and CD45$^+$/F4/80$^+$/CD4$^-$ macrophages. $N = 4$ mice for each genotype from two independent experiments.

X, Y Immunohistochemical staining of Ly6B.2 in WT and MyD88$^{\Delta PC}$ mouse ilea 4 d.p.i. Scale bars, 200 μm; 50 μm in high magnification images.

Z Numbers of Ly6B.2$^+$ cells per crypt-villus axis were counted and averaged from 10 different microscopic fields of three mice for each genotype. Data were analyzed by unpaired *t*-test.

Data information: All data represent mean ± SEM. *$P < 0.05$; **$P < 0.01$; ****$P < 0.0001$.
Source data are available online for this figure.

We found that *Salmonella* infection elevated ROS production and secretion in wild type mouse PCs. The observed dampening of gut inflammation in *MyD88$^{\Delta PC}$* mice may have indirectly reduced *Salmonella* virulence via above mechanism. However, the exact molecular impact exerted by *MyD88*-deficient PCs on the biology or virulence of *Salmonella* are not clear at this moment. Nevertheless, infected *MyD88$^{\Delta PC}$* mice had a reduction in Cd74$^+$ PCs, accompanied by reduced chemokines (e.g., CCL2 and CXCL1) in LP/PC co-culture, and a significantly reduced neutrophil recruitment. MyD88-dependent neutrophil recruitment has been reported in other tissues during infection and inflammation (Nance *et al*, 2008; Kirsebom *et al*, 2019). Thus, our observed reduction in chemokines likely account for the reduced neutrophils in *MyD88$^{\Delta PC}$* intestine. Therefore, loss of PC-specific MyD88 pathways dampened the inflammatory programs, such as releasing pro-inflammatory and complement-activating pentraxin, in these infection-stimulated PCs. This notion is supported by the observed reduction in complement activation and systemic infection in infected Mptx2 knockout mice. In addition to mediating TLR microbial sensing (Fitzgerald *et al*, 2001; Price *et al*, 2018), MyD88 is also implicated in signaling of IL-1 family cytokines (Adachi *et al*, 1998; Burns *et al*, 1998; Medzhitov *et al*, 1998; Kroeger *et al*, 2009). Receptors for these cytokines are indeed present in some PCs based on our scRNA data. These MyD88-dependent pathways known to modulate *Salmonella* infection susceptibilities via various cell type-specific mechanisms (Benjamin *et al*, 2013; Rauch *et al*, 2017) may also contribute to the observed phenotype in these mouse models.

An early microarray study reported elevated *CD74* in UC patient tissues (Lawrance *et al*, 2001). Increased CD74 abundances were found in colonic glands of IBD and experimental colitis, while global knockout of mouse Cd74 affected intestinal epithelial wound healing (Farr *et al*, 2020b). CD74 is a type II transmembrane protein first reported as the invariant chain of MHC class II complex (Schroder, 2016), however the expression of CD74 is widely distributed in immune cells and is independent of MHCII molecules (Henne *et al*, 1995). CD74 was later found to be the receptor for MIF (Bucala & Shachar, 2014). In steady state, most *Cd74*-expressing PCs are in the progenitor cluster that arises from stem cells. Our data showed that commensal microbiota failed to promote Cd74$^+$ PCs in germ-free mice, whereas infection stimulated their expansion. Based on our data, we believe that infection-stimulated Cd74$^+$ PCs can be a part of the intestinal epithelial response to invasive pathogens. Interestingly, Cd74$^+$ PCs are enriched with MIF (agonist of CD74), suggesting that upon activation, these PCs may propagate

the inflammatory cascades across the intestinal mucosal cell populations. Our results in aggregate suggest that infection or inflammation-activated cluster of PCs likely represent a key component of the innate immune circuit consisting resident LP and epithelial cells. In homeostasis, the low number of Reg3 or Mptx2-expressing PCs may serve as a basal surveillance, which can be expanded, activated to release proinflammatory molecules during pathogenic infection. Mptx2 contains a lectin domain, and along

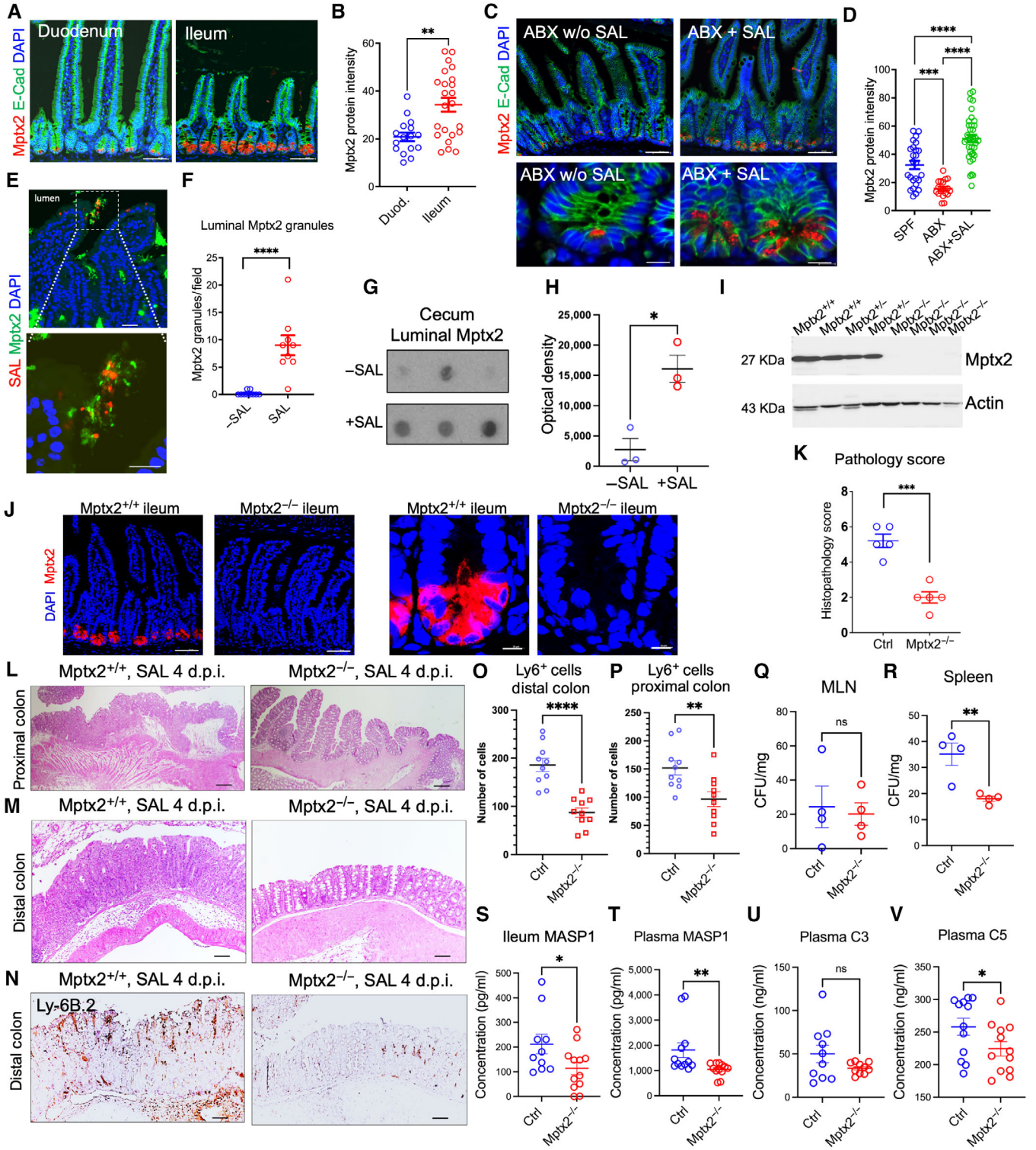

Figure 7.

Figure 7. Abolishing Mptx2, a Paneth cell-specific mucosal pentraxin, reduces complement activation.

A Immunofluorescent staining of Mptx2 (red) and E-Cadherin (green) in SPF mouse duodenum and ileum. Scale bars, 50 μm.
B Average Mptx2 fluorescent abundance per crypt was determined from 20 to 25 crypts imaged in six to eight independent fields for duodenum or ileum ($n = 5$ each) and compared by unpaired *t*-test.
C Immunofluorescent staining of Mptx2 (red) and E-Cadherin (green) in streptomycin-treated uninfected (ABX w/o SAL) and *Salmonella*-infected mouse ilea (ABX+SAL). Bottom panels are high magnification of crypts showing Mptx2 granules in ABX+SAL condition. Scale bars, 50 μm; 20 μm in high magnification images.
D Average Mptx2 fluorescent intensity per crypt was determined from 20 to 25 crypts imaged in six to eight independent fields for SPF, ABX or ABX+SAL mouse ileum ($n = 3$ mice per condition). One-way ANOVA was used to compare the differences.
E Immunostaining of Mptx2 (green) in *Salmonella* (red)-infected mouse ileum. White-boxed areas are shown in high magnifications to reveal luminal Mptx2 and *Salmonella* association. Scale bars, 20 μm; 10 μm in high magnification image.
F Numbers of luminal Mptx2 granules were counted and compared by unpaired *t*-test from five to eight independent fields of −SAL and +SAL mouse ilea ($n = 3$ mice per condition).
G, H Cecum luminal Mptx2 protein abundances were determined by dot blots in −SAL and +SAL mice ($n = 3$ mice per condition) and compared by *t*-test in panel (H).
I Western blots for Mptx2 were performed using ileal tissue lysates from WT ($Mptx2^{+/+}$), heterozygous ($Mptx2^{+/-}$), and homozygous ($Mptx2^{-/-}$) mice, all of which were littermates.
J Immunofluorescent staining of Mptx2 (green) in WT or $Mptx2^{-/-}$ mouse ileum. Scale bars, 50 μm; 10 μm in high magnification images.
K Hematoxylin & eosin (H & E) stained ileum, proximal and distal colons of WT or $Mptx2^{-/-}$ mice were scored 0–3 for degrees of epithelial damage, leukocyte infiltration into the mucosa, submucosa, and muscularis. Each score was multiplied by 1 (focal), 2 (patchy), or 3 (diffuse), and summed to obtain a final score per mouse. *t*-test was used for $n = 5$ mice of each genotype.
L, M Representative H & E stained proximal (panel L) and distal (panel M) colons of WT and $Mptx2^{-/-}$ mice 4 d.p.i. Scale bars, 200 μm.
N–P Representative immunohistochemistry for Ly6B.2 in WT and $Mptx2^{-/-}$ mouse distal colons 4 d.p.i. Average numbers of $Ly6B.2^{+}$ cells per colonic gland were compared by *t*-test from 10 fields of distal (panel O) and proximal (panel P) colons ($n = 4$–5 mice per genotype). Scale bars, 200 μm.
Q, R Mesenteric lymph node (MLN) and spleen *Salmonella* CFUs were counted, presented as per mg of tissue, and compared by *t*-test for WT ($n = 5$) and $Mptx2^{-/-}$ ($n = 4$) mice 4 d.p.i.
S–V ELISAs were performed for MASP1 proteins in ileum (panel S) and plasma (panel T), complement C3 protein (panel U) and C5 protein (panel V) in plasma from eight to 10 WT and $Mptx2^{-/-}$ biological replicates. Data were analyzed by *t*-test and represent mean ± SEM in two independent experiments.

Data information: All data represent mean ± SEM. $*P < 0.05$; $**P < 0.01$; $***P < 0.001$; $****P < 0.0001$.
Source data are available online for this figure.

with C-type lectins, they are potent activators of complement cascades. Their elevated productions during infection are conserved and likely designed as first line of defense to control infection. Our data suggest that $Cd74^{+}$ PCs may be promoted to fight against pathogens to control infection, however their stimulation of inflammation and recruitment of neutrophils are expected to exert collateral damages to host tissues.

It is plausible for different subsets of PCs to differentially modulate inflammatory cascades via crosstalk with resident immune cells, as suggested by recent works (Gaudino *et al*, 2021; Kamioka *et al*, 2022). The value of uncovering $CD74^{+}$ PCs is their presence in human intestinal disease tissues. When Cd74 conditional allele becomes available, future work is needed to delineate the responsible pathways regulating these PCs, the mechanism of expansion of these PCs, and their direct downstream targets. Taken together, our findings support a previous hypothesis that PCs may be a site of the origin for inflammation (Adolph *et al*, 2013) by identifying a candidate subgroup.

Materials and Methods

Human tissue biopsy

Analysis of 27 ulcerative colitis (UC), 41 Crohn's disease (CD), 13 celiac disease, 10 graft versus host disease (GvHD), and non-IBD resection tissues was approved by the Institutional Review Board of Washington University School of Medicine (IRB-201209047), Columbia University (IRB-AAAB2472, AAAS7061), Princeton Medical Center (IRB- BN2239; BN2294), and Cancer Institute of New Jersey (IRB-Pro20160001036). H.& E. sections of above human intestinal diseases were screened by GI pathologists at individual institutions. Sections were hand-picked for the presence of PCs in tissues of each specified disease.

Mice

All animal experiments were approved by the Institutional Animal Care and Use Committee (IACUC) at Rutgers University, Washington University School of Medicine, Rutgers New Jersey Medical School Comparative Medicine Resources, and Hackensack Meridian School of Medicine. Animal experiments were conducted in accordance with NIH guidelines and US federal laws. Mice were housed in individually ventilated cages under specific pathogen-free conditions, maintained on a 12-h light/dark cycle, and fed with food and water *ad libitum*. All experiments were performed on littermates that either contain wild type and knockout mice, or being randomly divided into treatment groups. At least three independent litters are used for each experimental comparison. Depending on intra-group variations, animal numbers are determined by power analysis to achieve meaningful statistical analysis. Experiments are typically repeated two to six times on different days.

To generate $Lyz1^{3'UTR\text{-}CreER}$ mice, a homologous recombination vector was constructed with the left arm (706 bp) inserted at *NotI* and *EcoRI* sites and the right arm (498 bp) inserted at *Mfel* and *HpaI* sites of a pIRES-CreERT2-Frt-PGK-*neo/kanR*-Frt vector. The vector was linearized by digesting at *NotI*/*HpaI* sites and electroporated into EL250 cells containing chloramphenicol-resistant RP23-92F3 BAC plasmid, and the recombined mutants were selected by kanamycin resistance. In addition, 0.2% Arabinose was subsequently added to the chloramphenicol-containing culture medium to activate Flpase expression for the depletion of the PGK-neo/kanR selection marker. Finally, the modified RP23-92F3 BAC containing $Lyz1^{3'UTR\text{-}IRES\text{-}CreER}$ allele was extracted and subjected to DNA

dialysis in microinjection buffer (10 mM Tris–HCl pH 7.4, 0.15 mM EDTA) using dialysis membrane (0.05 microns, type VM, Millipore). After dialysis, the DNA fragment was delivered to the Genome Editing Shared Resource of Rutgers-Cancer Institute of New Jersey, and injected into C57BL6/J embryos. After successful germline transmission, founders were screened through crossing with R26R-tdTomato mice (C57BL6, JAX# 007914) (Madisen *et al*, 2010). Genotyping primers for Lyz1$^{3'UTR\text{-}IRES\text{-}CreER}$ allele are 5′-CGGGCTCTACTT CATCGCATTCC3′ and 5′-ACACAGCATCAGCTGAAGCTTGTG′, which amplify a 347 bp product. These mice were crossed to *MyD88*$^{fl/fl}$ (C57BL6, JAX# 008888) (Hou *et al*, 2008) to develop PC-specific *MyD88* deletion. Deletion of floxed *MyD88* in PCs was confirmed by PCR using primers: 5′-CTGGGAGGCATCACCACCCTT and 5′-AGGCT GAGTGCAAACTTGGTCTGG, which amplify a floxed fragment.

For GvHD induction, C57BL/6 (B6, H-2^b, CD45.2$^+$, JAX# 000664) and BALB/c (H-2^d, JAX# 000651) were purchased from The Jackson Laboratory and housed at the animal facility at Hackensack Meridian School of Medicine. TNF$^{+/+}$ and TNF$^{DARE/+}$ mice (Kontoyiannis *et al*, 1999) of both sexes were maintained on a C57BL/6 background under specific pathogen-free conditions in Allentown caging on LabDiet 5010 chow (Purina, St. Louis, MO). To compare mouse duodenal and terminal ileal PCs, C57BL6/J mice (JAX# 000664) were sacrificed, and the entire length of the small intestine was harvested for PC and TEM analysis. CD74 KO mice on C57BL/6J background was developed (Bikoff *et al*, 1993) and described recently (Farr *et al*, 2020a). Mice were bred and maintained on a in specific pathogen-free conditions, maintained on a 12-h light/dark cycle, and fed with food and water *ad libitum*.

To derive gnotobiotic Lyz1$^{3'UTR\text{-}CreER}$;R26-tdTomato mice, a colony was shipped to the National Gnotobiotic Rodent Resource Center (NGCRR) at UNC – Chapel Hill, where sterile embryo transfer was performed. GF status of derived mice housed in Trexler isolators was validated by PCR and microbial culture at NGCRR. Fourteen mice were shipped in two separate shipments, and delivered to the Gnotobiotic Facility at Rutgers University in Taconic Germ-Free shippers. Following arrival, these mice were unpacked and housed in autoclaved gnotobiotic cages on ventilated racks (Allentown, PA) at a temperature-controlled gnotobiotic facility at Rutgers New Jersey Medical School. GF status was verified by IDEXX Laboratories, and monitored continuously by the facility using in-house protocols. All mice were maintained on a 12:12 light–dark cycle and fed an autoclaved non-purified diet.

Mptx2 KO mice were developed in the Genome Editing Shared Resource of Rutgers-Cancer Institute of New Jersey. Briefly, mouse C57BL/6J zygotes were electroporated with Cas9 protein (IDT) complexed with CRISPR sgRNA (MilliporeSigma). The sgRNA targeted the sequences 5′- AGATGCTATAAGGGCGAGTCAGG-3′ (PAM underlined) located in exon 2 of Mptx2; the target sequence is specific to Mptx2 gene but not to Mptx1. Founder mice were genotyped by PCR to detect the presence of insertion/deletions at the cut site using T7 Endonuclease I assay (NEB). Primers Mptx2A 5′-CAAATATCAGCATTGATAGG-3′ and Mptx2B 5′-TTCTTGTCCTA-GAATGATCT-3′ were used to amplify the DNA region overlapping CRISPR/Cas9 cut site. PCR products were sent for Next Generation Sequencing (Azenta Life Sciences). Founders with null mutations were used for breeding with C57BL6/J to establish Mptx2 KO lines. Founder #8, which was used for subsequent experiments, had a deletion 19 bp (TTCACAGACCTGACTCGCC) interrupting the coding sequence of exon 2. This line was verified for Mptx2 deletion at protein level. Genotyping primers: 5′CAAATATCAGCATTGATAGG3′ and 5′TTCTTGTCCTAGAATGATCT3′ amplify WT allele as 475 bp and KO allele as 456 bp fragments. All experiments involving animals were approved by the New Jersey Medical School Institutional Animal Care and Use Committee.

Bacterial strains

Salmonella typhimurium strain SL1344 was generously provided by Beth McCormick (University of Massachusetts Medical School). It was grown in Luria–Bertani (LB) broth with 100 μg/ml of ampicillin at 37°C. *Citrobacter rodentium* strain DBS100 (ATCC 51459) was grown in LB broth. *Clostridiodes difficile* strain VPI 10463 (ATCC 43255) and *R. gnavus* (ATCC, 29149) were anaerobically cultured in AnaeroGRO Chopped Meat Glucose Broth (Hardy Diagnostics, AG19H) at 37°C. *Lactobacillus rhamnosus* GG (ATCC, 53103) was cultured at 37°C in MRS broth (Fisher Scientific, Pittsburgh, PA, USA) following the manufacturer's protocol.

Paneth cell phenotype analysis

Lysozyme and human defensin 5 immunofluorescence were interpreted as described previously (Cadwell *et al*, 2008, 2010; Liu *et al*, 2014, 2016; VanDussen *et al*, 2014). For immunofluorescence, unstained slides were deparaffinized, followed by antigen retrieval using Trilogy (Cell Marque #920P-09; Rocklin, CA). Next, the slides were blocked with 1% bovine serum albumin and 0.1% Triton X-100 in phosphate buffer saline for 1 h before applying the primary antibody, defensin 5 (1:2,000; Novus, NB110-60002), overnight. After overnight incubation, secondary antibody donkey anti-rabbit (1:500; Life Technologies) was applied for 45 min, and slides were subsequently washed and stained with Hoechst (1:20,000; Sigma-Aldrich #33258). The stains were reviewed using an Olympus BX53 microscope equipped with an Olympus DP73 camera and cellSens Dimension software for adjusting brightness and contrast and image cropping.

S. typhimurium infection

A portion of the *S. typhimurium* SL1344 stab was inoculated in LB-ampicillin broth and grown at 37°C for 6 h, shaking. 10 μl of this culture was then used to inoculate 10 ml of LB-ampicillin broth and grown overnight at 37°C, without shaking. One-day post-i.p. injection of tamoxifen (75 mg tamoxifen/kg body weight), Lyz1$^{3'UTR\text{-}CreER}$; R26R-tdT mice were orally administered with 15 mg of streptomycin, followed by oral infection of PBS (ABX) or 10^8 CFU *S. typhimurium* (SAL) 24 h later. For *Salmonella* infection in non-PC reporter mouse lines, no tamoxifen was given to the mice. The mice were sacrificed 4 days after infection, and the ileum was harvested for crypt isolation or fixed in 10% buffered formalin for histological analysis. In addition, the cecal luminal content was collected and frozen at −80°C for dot blot analysis.

To compare the temporal PC labeling, in first cohorts of mice ($n > 20$), PCs were labeled before infection by injecting the reporter mice with tamoxifen prior to streptomycin and infection, while in post-infection cohort ($n = 4$), PCs were labeled after infection by

administering tamoxifen to a streptomycin-treated mice 1 day after infection. Four days post-infection, ileum was harvested for crypt isolation and subsequent FACS sorting.

For Lyz1$^{3'UTR\text{-}CreER}$; R26R-tdT; MyD88$^{L/L}$ (MyD88$^{\Delta PC}$) mice and wild type littermates sacrificed 4 days after infection, the body weight was monitored daily. On the day of sacrifice, mice were fasted for 2 h and orally gavaged with 600 mg/kg of 4 kDa fluorescein isothiocyanate (FITC)-dextran. After sacrifice, blood was collected by cardiac puncture vein bleed in EDTA-coated syringe, and serum FITC fluorescence was measured by a plate reader at an excitation wavelength of 495 nm to assess intestinal permeability. The harvested spleen and mesenteric lymph nodes (MLN) were homogenized and plated on XLD agar plates to determine the CFU of *S. typhimurium* disseminated to these organs. For histological analysis, ileum and colon tissues were harvested and fixed in 10% buffered formalin.

For Mptx2$^{-/-}$ and littermate wild type mice, mice were sacrificed 4 days after infection with daily body weight monitoring. Upon sacrifice, blood was collected by cardiac puncture for serum cytokine analysis. ~1 cm sections of the terminal ilea were collected for cytokine and protein-abundance analysis. Spleens, MLNs, and liver sections were homogenized and plated on XLD agar plates for *S. typhimurium* CFU determination. For histological analysis, ileum and colon tissues were harvested and fixed in 10% buffered formalin.

C57BL/6J microbiome colonization of germ-free Lyz1$^{3'UTR\text{-}CreER}$; R26R-tdT mice

Feces were collected from C57BL/6J mice housed in specific pathogen-free conditions. Feces were immediately placed in anaerobic chamber (Catalog #857-OTA, Plas Labs, Inc.) and homogenized in PBS. Germ-free Lyz1$^{3'UTR\text{-}CreER}$; R26R-tdT mice, housed at the gnotobiotic facility at Rutgers New Jersey Medical School and handled in a sterile gnotobiotic isolater, were orally gavaged 200 μl of the C57BL/6J fecal slurry once a week for 2 weeks.

Seventeen days after the initial fecal slurry gavage, the two mice who were colonized with C57/BL6J microbiome and two germ-free Lyz1$^{3'UTR\text{-}CreER}$; R26R-tdT mice were administered an i.p. injection of tamoxifen (75 mg tamoxifen/kg body weight). After 4 days, the mice were sacrificed and duodenum, jejunum, ileum, and colon tissues were harvested and fixed in 10% buffered formalin for histological analyses. For crypt isolation and single-cell dissociation, distal regions of the ilea were collected. For confirmation of colonization and germ-free status, feces were collected for DNA extraction and 16S qPCR analysis.

Mono-colonization of C57BL/6J germ-free mice by *R. gnavus* and *L. rhamnosus*

Ruminococcus gnavus and *L. rhamnosus* cultured broth was centrifuged at 1,200 *g* for 10 min to pellet the bacteria. On Day 0, adult C57BL/6J germ-free mice (Taconic) were gavaged with sterile PBS ($n = 5$ mice), 200 μl of *L. rhamnosus* ($n = 5$ mice) or *R. gnavus* ($n = 5$ mice) at a concentration of 10^8 CFU/ml resuspended in the same PBS solution. Colonization was validated by qPCR using strain specific primers. On Day 21, animals were sacrificed, and ileal tissues were used for RNA extraction using the RNeasy Plus Mini kit (Qiagen #74034). Same experiments were repeated for *L. rhamnosus* and *R. gnavus* mono-colonization each in a separate occasion, and ileal tissues were fixed for histology and immunostaining analysis.

DNA extraction and 16S qPCR

Feces were collected from the terminal colon of mice upon sacrifice. For DNA extraction, lysis buffer was adjusted by fecal weight and up to 800 μl was added per bead-containing tube following the manufacturer's instructions using Purelink Microbiome DNA Purification Kit (Invitrogen, Carlsbad, CA, USA). Samples were homogenized (30 s) in a bead homogenizer (Thermo Fisher, Waltham, MA) and centrifuged at 14,000 *g* (5 min), and the supernatants were collected in a 1.5 ml microcentrifuge tube (Eppendorf, Hauppauge, NY). Samples were transferred to a spin column for purification and eluted in 100 μl elution buffer (Invitrogen by Thermo Fisher). DNA concentrations were determined by spectrophotometry (Nanodrop, Wilmington, DL). Purified DNA was used for quantitative real-time PCR for 16S rRNA quantification in feces. The qPCR reaction was performed using SYBR Green (Thermo Fisher) as follows: 98°C for 3 min, followed by 50 cycles at 98°C for 10 s, 60°C for 30 s, and 72°C for 30 s, and a final extension at 95°C for 5 min, 60°C for 1 min, and 98°C for 30 s. Primers for the gene encoding 16S rRNA were as follows: 16S rRNA forward: 5′--ACTACGTGCCAGCAGCC-3′ and reverse 5′-GGACTACCAGGGTATCTAATCC-3′. No cycle threshold (Ct) values were detected for germ-free mice.

Crypt isolation and single-cell dissociation

The duodenum or ileum of tamoxifen-injected Lyz1$^{3'UTR\text{-}CreER}$; R26R-tdT mice was harvested, opened longitudinally, and cut into smaller fragments. The pieces were rinsed in cold PBS before shaking in 1× HBSS Ca/Mg-free (Sigma, Catalog No. H9394), containing 10 mM EDTA (Invitrogen, AM9260G) for 10 min at 4°C. The tissues were then transferred to fresh 10 mM EDTA-HBSS medium for 30 min at 4°C. After vigorous shaking, the flow-through collected from 70-μm filtering was centrifuged at 700 *g* for 5 min at 4°C. Next, the pellet was resuspended with TrypLE Express (Thermofisher, 12605028) containing 0.5 mg/ml of DNaseI (Qiagen, 79254) for no more than 18 min at 37°C. Next, the cell suspension was passed through a 40-μm filter, centrifuged at 700 *g* for 5 min at 4°C, and resuspended in FACS buffer (F12/DMEM containing 2 μM ROCK inhibitor, 2% BSA, 2% FBS, and 2 mM EDTA).

Intestinal crypt isolation and *ex vivo* culture

The procedure for Intestinal crypts isolation was previously described (Yu *et al*, 2014, 2018). Intestinal crypts isolated from Lyz1$^{3'UTR\text{-}CreER}$; R26R-tdT mice were counted and resuspended in Matrigel (Corning, Catalog No. 354230). After Matrigel polymerization, IntestiCult organoid growth media (StemCell Technologies, Catalog No. 06005) was added to each well. After 6 days, 4-OHT (0.5 μM) was added to the media for 24 h. Images of viable enteroids were taken up to 4 days after 4-OHT treatment, using the Nikon Eclipse80i microscope and DS-Ri1 digital camera, and analyzed by ImageJ.

Staining and FACS sorting

The isolated crypt single epithelial cells were stained with DAPI and subjected to sorting by BD Biosciences Aria II Flow Cytometer (BD FACSAria II) for single-cell RNA sequencing. To assess levels of reactive oxygen species generated, isolated crypt cells were incubated with 500 nM of CellROX Green reagent (ThermoFisher, C10444) for 30 min at 37°C, followed by sorting after one wash with FACS buffer. For analysis of live cells, cells were resuspended with FACS buffer containing anti-mouse Fc (1:100; BioLegend, 101330) for 10 min on ice. After centrifugation, these cells were stained with surface markers on ice for 30 min. The live cells were then centrifuged, stained with DAPI, and subjected to analysis. Similarly, for analysis of fixed cells, cells were resuspended with FACS buffer containing Live/Dead 488 (1:200; ThermoFisher, L34969) or Live/Dead 405 (1:200; ThermoFisher, L34963) and anti-Fc (1:100) for 10 min at room temperature, followed by staining with surface markers on ice for 30 min. Next, the cells were centrifuged, fixed with 1% PFA on ice, and sorted. When staining for intracellular markers, the surface-stained cells were fixed (ThermoFisher, 00552300) for 30 min on ice, followed by incubation with antibodies for intracellular markers in permeabilization buffer (ThermoFisher, 00552300) overnight at 4°C. The next day, cells were incubated with secondary antibodies against Gpx2 and RFP for 1 h at room temperature. Finally, the cells are spun down and resuspended in the FACS buffer before analysis.

The following surface markers were used – PerCP/Cy5.5-conjugated EpCAM (1:200; BioLegend, 118219), APC/Fire750-conjugated CD24 (1:200; BioLegend, 101840), and AF647-conjugated CD74 (1:100; BioLegend, 151004). These intracellular markers were used- Gpx2 (1:100; Santa Cruz Biotech, 133160), CD74 (1:100; R & D, AF7478), and RFP (1:200; Rockland, 600401379). The following secondary antibodies were used – donkey anti-rabbit AF555, donkey anti-mouse AF405, or donkey anti-sheep AF488. For all fluorophores, a cell pellet was stained with a single antibody (of all primary antibodies used) and compared to unstained pellet to determine compensation controls.

Single viable PCs were gated by forward scatter, side scatter, negative staining for DAPI or Live/Dead marker, and positive staining for tdTomato (using PE channel) or RFP. Subpopulations were further gated based on EpCAM, CD24, CD74, GPX2, or CellROX. Sorted tdT^+ or RFP^+ viable singlets were further analyzed by Millipore Amnis ImageStream Imaging Flow Cytometer (ImageStream X Mark II) or centrifuged at 700 *g* for 5 min for cytokine array or dot blot analysis. All flow cytometric data were analyzed using Flowjo software (TreeStar, version 10.7.1). Amnis Imaging data were visualized by IDEAS software (Millipore, version 6.2). All antibodies and key reagents are detailed in Appendix Table S1.

Proteome profiling of PC secretome

For secreted protein analysis of $CD74^+$ PCs, $tdT^+/CD74^+$ cells were flow-sorted from three reporter mice, pooled, and centrifuged. Cell pellets were resuspended in RPMI-1640, containing glutamine, 10% FBS (Sigma, F2442), 1× Penicillin/Streptomycin (ThermoFisher, 15140122), 20 mM HEPES (ThermoFisher, 15630080), 1× MEM non-essential amino acids (ThermoFisher, 11140050), 1 mM sodium pyruvate (ThermoFisher, 11360070), and 50 μM β-mercaptoethanol and seeded into a 24-well plate. Wells with culture medium only were used as blank control. Sixteen hours later, culture media was collected and centrifuged at 1,000 *g* for 5 min. The cytokines in the supernatant were measured using the Proteome Profiler™ XL Mouse cytokine array kit (R&D systems, ARY028), and the procedure was performed according to the manufacturer's instructions. Dot intensity was determined by Image J, and the values from blank medium control was subtracted. The resulting data were natural log transformed to present on a radar chart. Radar plots were constructed through the FMSB package in R.

Droplet-based single-cell RNA-seq

Cell number and viability were determined by a propidium iodide-based fluorescence assay using Moxi GO II System, Orflo Prod#MXG102 (ORFLO Technologies, LLC). Droplet-based single-cell partitioning and single-cell RNA-Seq libraries were generated using the Chromium Single-Cell 3′ Reagent v3 Kit (10× Genomics, Pleasanton, CA) on the 10× Chromium Controller as per the manufacturer's protocol. Live cells in single-cell suspension with 95% viability were mixed with Gel beads, RT reagents, and Partitioning Oil into a Single-Cell 3′ Chip and loaded onto a 10× Chromium Controller for GEM generation. Briefly, the protocol includes RT, cleanup, cDNA amplification, fragmentation, end repair and A-tail prep, adapter ligation, and incorporation of sample indices into finished libraries, which are compatible with Illumina next-generation sequencing platforms. Sample quantification and quality control were determined using Qubit Fluorometer (Invitrogen, Life Technologies) and TapeStation (Agilent Technologies, Santa Clara CA), respectively. cDNA libraries were sequenced on Illumina NovaSeq 6000 sequencer (Illumina, San Diego, CA) with a configuration of 28/8/0/91-bp for cell barcode, sample barcode, i5 index, and mRNA reads, respectively, as a recommendation by 10× Genomics. The Chromium Single Cell Software is used to analyze and visualize single-cell 3′ RNA-seq data produced by the 10× Chromium Platform. The 10× Chromium software package includes Cell Ranger Pipelines and Loupe Cell Browser. Cell Ranger pipelines use raw 10× single-cell sequencing data from an Illumina sequencer and perform demultiplexing, unique barcode processing, and single-cell 3′ gene counting.

Condition	Estimated number of cells	Mean reads per cell	Median genes per cell
Duo-SPF	6,626	73,044	1,237
Ile-SPF	6,893	79,440	1,079
Ile-ABX	8,352	62,881	1,323
Ile-SAL	8,178	60,926	1,306
GF ileum	5,224	95,168	2,388
GF+B6M ileum	5,646	92,455	2,382

Seurat-based computational analysis

The count matrix files generated by Cell Ranger were transformed into the count matrix by R (version 4). Count matrices for different groups were combined and used as the input for Seurat package

(version 4) (Butler *et al*, 2018; Stuart *et al*, 2019). Cells with fewer than 200 unique feature counts and genes that are expressed in fewer than three cells were considered as the low-quality measurements and filtered out. Cells having > 20% mitochondrial counts over a low total UMI count likely represent the dead cells, and were filtered out. To exclude doublets/multiplets, we filtered out cells double the mean UMI counts of all cells: in this case nine cells were above the threshold. The counts were normalized by library size, log-transformed, and scaled with the default setting of Seurat. The top 2,000 highly variable genes were used to perform PCA (principal component analysis). Ten of 20 principle components were selected for doing clustering and Uniform Manifold Approximation and Projection (UMAP). DE (differential expression) was performed by Seurat using the Wilcoxon test and visualized as dot plots or violin plots. fGSEA analysis was performed by Seurat using *fGSEA* tool for hallmark and reactome pathways.

For analysis of germ-free tdT$^+$ PCs: Given the read count matrices, data filtering, transformation, and dimensionality reduction were performed using the Seurat package (Stuart *et al*, 2019) following its standard analysis pipeline. Genes that were expressed in fewer than 3 cells and cells with fewer than 200 detected genes were filtered out. The principal component analysis was performed using default settings in Seurat. When calculating the UMAP coordinates, the first 20 principal components were used. The clustering analysis was performed using the FindClusters function with a resolution parameter of 0.2. In panels (G–L), the gene expression levels are presented as the normalized expression by Seurat.

Slingshot analysis

The Slingshot method (Street *et al*, 2018) was applied to carry out the trajectory analysis. The UMAP coordinates and cluster labels calculated by Seurat were used as the input of Slingshot to infer lineages. Based on the input information, Slingshot would identify lineages by treating the clusters of cells as nodes in a graph and constructing a tree between these nodes. For each lineage, Slingshot could calculate a pseudotime variable for every cell to represent the relative ordering of the cell in the lineage. The pseudotime variables for the first lineage was used for visualization in the figure.

Single cell deep constrained clustering (scDCC)

Single cell deep constrained clustering was performed for on SPF, ABX, and SAL datasets based on Cd74 expression. The top 2,000 most highly variable genes were identified using Seurat with the selection method of "vst" that calculates feature variance by fitting the variance–mean relationship. Then the expression data of these genes was fed to scDCC. scDCC is a deep learning model that requires two inputs: expression data and marker genes. In this study, scDCC was based on marker Cd74. The restriction of binding genes was based on their distances from each other. If the distance between two genes was among the top 10% farthest distances, they were marked as not being connected, while if their distance was smaller than 90% of distances of other gene pairs, they were marked as must be connected. After scDCC reduced the dimensions of the scRNA-seq data, t-SNE was applied for visualization. *Cd74*$^+$ cells were identified as those with *Cd74* reads ≥ 1 per cell and *Cd74*$^-$ were identified as cells with no reads of *Cd74*.

Highlighting fGSEA pathways on UMAP using cutoff

After datasets were normalized by Seurat, to demonstrate pronounced differences in expression levels of markers in cells, the following normalization was performed.

$$zi = \frac{(xi - \min(x))}{(\max(x) - \min(x))}$$

where zi is the ith normalized value in the dataset, xi is the ith value in the dataset, min (x) is the minimum value in the dataset, and max (x) is the maximum value in the dataset.

Some cells had relatively higher expression levels of indicated genes, so we set a threshold value to visualize the data better. Therefore, the highest threshold of cells was set at 95%, and all the cells above this threshold would have the same expression value. The upper expression range in these UMAPs will be denoted as "1+".

Cell–cell correlation matrix

To identify heterogeneity among SPF PCs, Duodenum (D) and Ileum (I) datasets were first normalized and dimensionally reduced by Seurat. The cells were then ranked in decreasing order by the sum of the normalized expression value of the genes highlighted by each PC subsets. Based on the principal component analysis (dimension = 20), the correlation was computed using the R function cor. The correlation was visualized as a heatmap (cells by cells) using the R package pheatmap (Hu, 2021), where the color reflected the correlation value.

Gene expression correlation of PCs across different studies

Single-cell transcriptome data of mouse and human ileal PCs were obtained from Gene Expression Omnibus (GEO) GSE92332 (Haber *et al*, 2017) and GSE125970 (Wang *et al*, 2020b). Expression data of ileal PCs from the three studies were normalized by Seurat. The differences in gene expression were visualized by jittered point plot, where each dot represents a cell. The data set in this study had more cells with non-zero expression values than other studies.

Clostridiodes difficile and *Citrobacter rodentium* infection

Clostridiodes difficile from a frozen glycerol stock was inoculated and grown overnight in AnaeroGRO Chopped Meat Glucose Broth at 37°C. After 24 h, the culture reached an OD_{600nm} of 2.14. It was centrifuged at 1,200 *g* for 5 min and resuspended in sterile PBS to prepare an inoculum of 4×10^6 CFU. A WT mouse was administered with tamoxifen 1 day before being treated with 0.5 mg/ml of cefoperazone. The mouse was given cefoperazone in their drinking water for 5 days, followed by 2 days of plain water (Fletcher *et al*, 2021). After which, the mouse was orally gavaged with 4×10^6 CFU of *C. difficile*, and sacrificed 2 days post-infection.

Luria–Bertani broth was inoculated with *C. rodentium* from a frozen glycerol stock and grown overnight at 37°C. At an $OD600_{nm}$ of 2.66, 5 ml of fresh LB broth was inoculated with 50 µl of overnight culture. This culture grew for 3 h at 37°C to an $OD600_{nm}$ between 1 and 1.5. The required volume of culture was then centrifuged at 1,200 *g* for 5 min and resuspended in sterile PBS to orally gavage a tamoxifen-injected WT mouse with 1.7×10^9 CFU of *C. rodentium* (Wang *et al*, 2020a). The mouse was sacrificed 4 days after infection.

A tamoxifen-injected WT mouse served as the uninfected control. The ileum of these mice was harvested for crypt isolation or fixed in 10% buffered formalin for histological analysis post-infection.

GvHD induction

Mice underwent bone marrow transplantation and GVHD induction as described (Zhang *et al*, 2002). In brief, we irradiated BALB/c recipients to 850 cGray from an X-Ray source followed by transplantation with donor B6 T-cell-depleted BM cells (5×10^6) mixed with or without $CD4^+$ T cells ($0.5–0.75 \times 10^6$). Donor BM cells were depleted of T cells using CD4 positive purification beads (Miltenyi, 130-117-043) and CD8 positive purification beads (Miltenyi, 130-117-044). Donor T cells were isolated using the enrichment CD4 microbeads (Miltenyi). GvHD scores and severity were graded according to clinical parameters and histopathological analysis, as described (Zhang *et al*, 2011; He *et al*, 2012). Five to six mice were used for each time point reported in the results. For correlation analysis, each of the GvHD mice (day 22 and 38) with variable inflammatory severities were microscopically scored for degrees (0–3) of epithelial damage, immune cell infiltration to mucosa and submucosa, as well as the percentage of $CD74^+$ PCs out of all PCs. The correlation plot was generated and correlation coefficient (r) calculated by Graphpad Prism.

RNA BaseScope assay

The BaseScope *in situ* hybridization (ISH) assays were performed following the manufacturer's instructions (Advanced Cell Diagnostics, ACD, Newark, CA). In brief, formalin-fixed-paraffin-embedded sections (5 μm) were used for mRNA detection using the BaseScope Duplex Detection Reagent Kit. For protease treatment, Protease III was used for 15 min incubation at 40°C. C2 probe was diluted in C1 probe at a 1:200 ratio. For step Hybridize BaseScope Duplex Amp7 and Amp11, incubation with reagent was limited to 5 min and 40 min, respectively. The tissues were counterstained with 50% Gill #2 hematoxylin (Sigma Aldrich, St Louis, MO) and then treated with 0.02% ammonia water. The slides were air-dried before adding a drop of Vectamount mounting medium (cat. H-5000). To minimize variation due to staining conditions, tissue samples were processed simultaneously and considered a replicate set. Images were captured and analyzed using a Nikon Eclipse80i microscope and DS-Ri1 digital camera. The ISH staining was quantified using the deconvolution tool in Image J. For quantification of human tissues treated with CD74 and LYZ Basescope probes, the number of CD74 transcripts per LYZ^+ PC were counted from three to six images of each patient, and the averages were graphed for individual patients. In addition, the percentage of $CD74^+/LYZ^+$ cell number over LYZ^+ cell number per patient was graphed for individual patients. Probes for human tissues were designed as follows: a 3zz pair probe name BA-Hs-CD74-tv1-3EJ-C1 targeting 264–547 bp of NM_001025159.3, and a 3zz pair probe named BA-Hs-LYZ-3EJ-C2 targeting 133–418 bp of NM_000239.3.

Isolation of lamina propria cells

The lamina propria cells (LPs) were isolated as previously described (Yu *et al*, 2020). The distal ileum of mice mentioned was dissected and briefly rinsed in ice-cold PBS (Fisher Scientific, SH30256LS). Next, the tissue was opened longitudinally, rinsed in ice-cold PBS, and further sliced to 2–3 mm pieces. These pieces were rinsed in 30 ml of ice-cold PBS by inverting the falcon tube 10–15 times and then transferred into fresh 30 ml of ice-cold PBS. This step was repeated until the solution remained clear after inverting. Each piece was then transferred to a 30 ml crypt isolation buffer containing 5 mM EDTA (Invitrogen, AM9260G) in HBSS Ca/Mg-free (Sigma, Catalog No. H9394), and allowed to shake at 37°C for 15 min. The tubes were subsequently vigorously shaken to release the epithelial layer from the pieces, after which the solution was discarded. Next, the tissues were transferred into another 30 ml of crypt isolation buffer to shake for 15 min at 37°C. The pieces were then incubated in DMEM/F12 medium (ThermoFisher, 12634-010) for 10 min on a petri dish at room temperature. The solution was discarded, and the pieces were thoroughly minced. Next, 10 ml of RPMI-1640 with glutamine (Fisher, MT10040CM) containing 100 U/ml Collagenase II (ThermoFisher, 17101015), 500 U/ml DNase I (Sigma, DN25), and 2% BSA (Sigma, A3294) was added to the minced tissue, and allowed to shake at 37°C for 30 min. The solution was passed through a 70 μM cell strainer into a 50 ml falcon tube when tissues were digested entirely. The tubes were centrifuged at 200 *g* for 10 min. For FACS analysis of LPs, the pellet was stained with specified antibodies (see Section Lamina propria cell flow cytometric staining).

Ex vivo co-culture of lamina propria and PCs

For *ex vivo* culture, LPs were isolated as described above. Cell pellet was resuspended in RPMI-1640, containing glutamine, 10% FBS (Sigma, F2442), 1 × penicillin/streptomycin (ThermoFisher, 15140122), 20 mM HEPES (ThermoFisher, 15630080), 1 × MEM non-essential amino acids (ThermoFisher, 11140050), 1 mM sodium pyruvate (ThermoFisher, 11360070), and 50 μM β-mercaptoethanol and seeded into 24-well plate.

Live tdT^+ PCs were sorted and collected from *S. typhimurium*-infected streptomycin-treated WT and $MyD88^{\Delta PC}$ mice ($n = 3$ for each genotype), and pooled per genotype. Wells containing LP mono-culture were used as controls (without PCs), 5,000 tdT^+ PCs from WT or $MyD88^{\Delta PC}$ mice were seeded to each wells containing equivalent LP cells. In a different set of experiments, live $Cd74^+$ and $Cd74^-$ tdT^+ PCs were sorted and pooled from three *S. typhimurium*-infected reporter mice. 5,000 $Cd74^+$ or $Cd74^-$ tdT^+ PCs were added to LP wells, with LP mono-culture wells (without PCs) serving as controls.

After 16 h of co-incubation, the culture media was centrifuged at 1,000 *g* for 5 min. The cytokines in the supernatant were measured using the Proteome Profiler™ mouse cytokine array kit (R&D systems, ARY006), and the procedure was performed according to the manufacturer's instructions. Two experiments were performed for each co-culture assays, and all experiments were performed under the same conditions to reduce the variabilities. The images of the immunoblots were analyzed by Image J to quantify the signal of each cytokine from two duplicate dots. The intensity of each cytokine was normalized against the dot blots of LP monoculture used in the same experiments. The ratio was log transformed and used to plot on radar charts using Origin Pro 2019 (https://www.originlab.com).

MIF, 4-IPP, and CD74 neutralizing antibody treatment

Live tdT$^+$ cells were sorted as described earlier. 30,000 tdT$^+$ PCs were sorted into four eppendorfs containing 200 μl of the nutrient-enriched medium. Cells in tube 3 were incubated with 10 μg/ml of anti-CD74 antibody (Santa Cruz Biotech, sc-6262) to block CD74, while cells in tube 4 were incubated with 100 μM of 4-IPP (Millipore Sigma, 475846) (Bozzi *et al*, 2017), a MIF antagonist, for 10 min at room temperature. Cells in tubes 2, 3, and 4 were then treated with 100 ng/ml of recombinant MIF (R & D systems, 1978-MF-025) for 20 min at room temperature. After centrifugation, the supernatant was collected for dot blot analysis while the cells were incubated with 500 nM of CellROX Green reagent (ThermoFisher, C10444) for 30 min at 37°C. These cells were then washed with FACS buffer and analyzed by flow cytometry.

Immuno-dot blot analysis

Fecal pellets from wild type SPF mice of different ages (postnatal day 10–15, 1-month old, and over 1 year old) were weighed and snap frozen at −80°C. Cecal contents were collected from uninfected and *Salmonella*-infected mice of various genotypes described in results. To prepare fecal protein extraction, these samples were sonicated in 1 × PBS containing protease inhibitor cocktail tablet (Sigma, 1183617001), and centrifuged at 4°C for 15 min at 18,000 RCF. The protein concentration of the supernatant from each sample was determined by BCA assay. 40 μl of 1 μg/μl sample prepared with 1× Protease inhibitor cocktail tablet and 4 μl of β-mercaptoethanol, were denatured at 95°C for 5 min. Prior to loading the samples on a 96-well dot blot apparatus, 100 ml of 1× TBST was added to equilibrate each well. After the TBST was absorbed, samples were loaded onto the apparatus and left to dry overnight. The next day, the membrane was removed from the apparatus and incubated in TBST for 5 min, followed by blocking with 5% milk in TBST solution for 1 h. The membrane was incubated with a specified primary antibody at 4°C overnight. After washing with 1× TBST three times for 30 min each, the membrane was incubated with a secondary antibody for 1 h at room temperature. The membrane was finally developed with ECL detection reagent (VWR, 89168-782) after washing with 1× TBST three times for 30 min each. The density of dot was quantified by ImageJ's region of interest (ROI) tool, followed by subtraction of the background intensity from the spot's pixel intensity. Same procedure was used to detect Mptx2 from secretome of *ex vivo* cultured or stimulated PCs, except that the denatured culture supernatant was loaded instead of the fecal protein extracts.

Bulk RNA-seq data analysis

The bulk RNA-seq of mouse ileum was analyzed on the CLC Workbench version 20.04. Mapping was performed using the *Mus musculus* reference genome and transcript sequence from Ensembl (GRCm38) on trimmed reads (80 bp average read length). TPM counts were generated and used for heatmap generations by utilizing the *pheatmap* package on R. The fragments per kilobase million (FPKM) values were normalized and plotted in bar graphs or on a heatmap.

Lamina propria cell flow cytometric staining

Lamina propria cells were isolated from the distal ileum as described earlier. The LP pellet was resuspended in 1 ml of 10% FBS in PBS and centrifuged at 300 *g* for 5 min at 4°C. Cells were resuspended in 100 μl of FACS buffer (2% BSA in PBS) containing anti-Fc (1:100) on ice for 10 min. After centrifugation, cells were incubated with FACS buffer containing anti-Fc (1:100) and Live/Dead 405 (1:200; ThermoFisher, L34963) for 5 min at room temperature. Cells were then washed with 1 ml of 10% FBS in PBS and centrifuged at 300 *g* for 5 min at 4°C. Cell pellets were then resuspended in 100 μl of surface staining solution containing the following antibodies: anti-Fc (1:200), CD45 BUV395 (1:200, BD Biosciences, 564279), CD4 BV510 (1:100, Biolegend 100553), TCRβ APC/Cy7 (1:100, BioLegend, 109219), MHCII AF647 (1:200, BD Biosciences, 562367), CD11c BV786 (1:200, BD Biosciences, 563735), CD103 AF594 (1:100, BioLegend, 121428), F4/80 PerCP/Cy5.5 (1:100, BioLegend, 123128), CX3CR1 BV711 (1:100, BioLegend, 149031), and Ly6G AF488 (1:200, BioLegend, 127625). Cells were incubated with staining solution for 30 min on ice followed by a wash with 1 ml of FACS buffer and centrifuged at 300 *g* for 5 min at 4°C. Pellet was resuspended in 1% PFA in FACS buffer and analyzed on BD Biosciences Aria II Flow Cytometer (BD FACSAria II). For all fluorophores, control cell pellets were stained with single antibodies and compared to unstained pellet to determine compensation controls.

Enzyme-linked immunosorbent assays (ELISA) for complement activity determination

Mouse MASP1 ELISA Kit (Abcam, ab272473), Mouse Complement C5 ELISA Kit (Abcam, ab264609), and Mouse Complement C3 ELISA Kit (Abcam, ab157711) were used per manufacturer's protocol on mouse plasma or ileum lysates. Plasma was isolated via cardiac puncture in EDTA-coated syringe, and blood was centrifuged at 3,000 *g* for 5 min. For C5 analysis, a 1:33 plasma dilution was used; for MASP1 analysis, a 1:200 dilution of plasma was used, and for C3 analysis, a 1:50,000 dilution of plasma was used. For ileal tissue analysis, distal ileum was isolated and weighed. 10 μl of lysis buffer (50 mM Tris–HCl pH 7.5, 150 mM NaCl, 10 mM EDTA, 0.02% NaN_3, 50 mM NaF, 1 mM Na_3VO_4, 1% NP-40, 1 mM PMSF, 0.5 mM DTT, commercial protease and phosphatase inhibitors [Millipore Sigma, 11697498001 & 4906837001]) per mg of tissue was added and tissues were sonicated, followed by centrifugation at 12,000 *g* at 4°C for 10 min. Supernatants were isolated and dilutions of ileal tissue lysates used for each ELISA kit are as follows: C5, 1:6.67 dilution; MASP1, 1:3.3 dilution; and C3, 1:200 dilution.

Peroxidase activity assay

tdT$^+$ cells sorted from *Salmonella*-infected WT ileum were resuspended in FACS buffer with or without 100 ng/ml of recombinant MIF (R & D systems, 1978-MF-025) for 30 min at room temperature. Cells were then centrifuged, and the supernatant was collected. QuantiChrom™ Peroxidase Assay Kit (Bioassay Systems, Cat#D2PD-100) was used to analyze the peroxidase activity in each sample. Briefly, supernatant samples were diluted by a factor of 10, and

10 µl of each sample was loaded on a black flat-bottom plate and incubated with 90 µl of assay reagent (electron donor dye, 0.6% hydrogen peroxide, and assay buffer) for 10 min at room temperature. Samples were subjected to fluorescence measurement (Ex/Em = 530/585 nm) and the peroxidase activities (units/l) were calculated as follows:

$$\text{Peroxidase activity} = \frac{R_{SAMPLE} - R_{BLANK}}{R_{RESORUFIN} - R_{WATER}} \times \frac{[\text{RESORUFIN}]\,(\mu M)}{t\,(\text{min})} \times \frac{\text{Reaction volume}\,(\mu l)}{\text{Sample volume}\,(\mu l)} \times 10.$$

R_{SAMPLE}, R_{BLANK}, $R_{RESORUFIN}$, and R_{H2O} are the fluorescence readings of the sample, sample blank, Resorufin, and water, respectively. The Resorufin concentration was 5 µM and the reaction volume was 100 µl.

Tissue collection, fixation, and immunofluorescence

Mouse intestinal tissues were fixed in 10% neutral formalin overnight, transferred to 70% ethanol the next day, and embedded in paraffin at the Histology Core Facility at Rutgers New Jersey Medical School. Then, 5-µm sections were sliced from paraffin blocks, rehydrated, and subjected to H & E staining. $TNF^{+/+}$ or $TNF^{DARE/+}$ mice (all on C57BL6/J) were euthanized at 4, 8, 10, and 17 weeks of age (n = 5 of each time point), and the ileum was fixed in 10% neutral buffered formalin, paraffin-embedded, and sectioned.

The procedures for immunofluorescence have been previously described (Yu *et al*, 2018). Briefly, the slides were rehydrated, subjected to antigen retrieval (citrate acid buffer, pH 6), and incubated in the blocking buffer (PBS containing 0.1% Triton X-100 with 2% normal serum and 2% BSA) at room temperature for 1 h. Then the slides were probed with the primary antibodies at 4°C overnight. The primary antibodies used on mouse tissue were- Sheep anti-CD74 (R & D, AF7478), Rabbit anti-Lysozyme (BioGenex, AR024), Rabbit anti-RFP (Rockland, 600-401-379), Mouse anti-E-Cadherin (BD Biosciences, 610404), Rabbit anti-Mptx2 (Abcam, ab238123), Mouse anti-*Salmonella typhimurium* (Santa Cruz Biotech, sc-58026), or Mouse anti-PCNA (Santa Cruz Biotech, sc-56). In comparison, the human tissues were stained with Mouse anti-CD74 (ThermoFisher, PA5-22113), Rabbit anti-Lysozyme (BioGenex, AR024), Rabbit anti-alpha Defensin 5 (Novus Biologicals, NBP1-84282), or Goat anti-MMP7 (Santa Cruz Biotech, sc-8832). Next day, these slides were then incubated with Alexa Fluor-conjugated secondary antibodies for 1 h at room temperature, followed by staining with DAPI. Slides were mounted with Prolong Gold Antifade Mountant (Invitrogen, P36930). Images were collected using confocal ZEISS LSM980 with Airy Scan and LSM510, and analyzed by ImageJ or Zen software. The Cd74 antibody and Mptx2 antibody were both validated by us on corresponding knockout mice.

Pathology score of intestinal inflammation

Inflammation was blindly scored as described previously (Chassaing *et al*, 2014). H & E-stained ileal and colonic section was assigned 4 scores of (0–3) based on degree of epithelial damage, leukocyte infiltration into the mucosa, submucosa, and muscularis/serosa. Each of the four scores is multiplied by 1 for focal, 2 for patchy, and 3 for diffuse, and summed to achieve the final score per mouse.

Transmission electron microscopy

The procedure for transmission electron microscopy was described previously (Gao & Kaestner, 2010; Yu *et al*, 2014). Briefly, pellets of untreated crypts, crypts treated with recombinant mouse MIF, and crypts treated with 4-IPP and MIF were fixed in 0.1 M sodium cacodylate containing 2% glutaraldehyde (EM grade) and 2% paraformaldehyde (EM grade) overnight fixation at 4°C. The next day, samples were washed twice with 0.1 M sodium cacodylate, then post fixed with 1% buffered OsO4 and stained with 1% uranyl acetate. Next, these samples were dehydrated using increasing concentrations of ethanol, followed by propylene oxide. The samples were further infiltrated with EMBed-812/propylene oxide (1:1) and 100% EMBed-812, after which they were embedded using the EMBed-812 kit (Electron Microscopy Sciences, Catalog No.14120).

Fecal bacterial DNA extraction, 16S sequencing, and analysis

DNA was extracted from stool samples of separately housed WT and Mptx2-KO mice, using QIAamp PowerFecal Pro DNA Kit (QIAGEN, Hilden, Germany), and analyzed by 16S amplicon profiling. The hypervariable V4 region of the 16S rRNA gene was amplified from each sample with unique barcoded reverse primers (806R) and forward primer (515F) using MyFi™ Mix (Bioline Meridian, Cat No. BIO-25050). Both reverse and forward primes were extended with the sequencing primer pads, linkers, and Illumina adapters (Caporaso *et al*, 2012). PCR was performed using the LightCycler 96 (Roche) in the final volume of 40 µl. Amplicons were quantified using Quant-It PicoGreen dsDNA Assay kit (ThermoFisher Scientific, Cat No. P7589), according to the manufacturer's protocol. Equal amounts of 240 ng of amplified DNA from each sample were pooled and cleaned using UltraClean PCR Clean-Up Kit (QIAquick PCR Purification Kit, Qiagen, Cat No. 28104). Pooled amplicons were diluted and denatured with 0.2 N NaOH. The library was sequenced at the University of Arizona PANDA CORE for Genomics and Microbiome Research using the MiSeq platform (Illumina) and custom sequencing primers (Caporaso *et al*, 2012). Due to the limited sequence diversity among 16S rRNA amplicons, 5% of the PhiX Sequencing Control V3 (Illumina, Cat No. FC-110-3001) made from phiX174, was used to spike the library and increase the diversity.

The raw sequencing data were demultiplexed using the *idemp* script (https://github.com/yhwu/idemp). Filtering, dereplication, chimera identification, and merging of paired-end reads were performed with dada2 (Callahan *et al*, 2016). The Amplicon Sequence Variants (ASVs) taxonomy was assigned using the Ribosomal Database Project (RDP) classifier (Wang *et al*, 2007) against SILVA database release 138 (Quast *et al*, 2013). Taxonomic richness and evenness (Shannon and Simpson indices) were calculated and statistically analyzed using T-test. Differences in microbial communities were evaluated using non-metric multidimensional scaling (NMDS) ordination analysis on Bray–Curtis distances followed by permutational multivariate analysis of variance (PERMANOVA) to analyze the contribution of the genotype to microbial community composition dissimilarities. The obtained results were visualized

with a *ggplot2* (ver 3.3.2) package (Wickham, 2016) and figure assembled in Microsoft PowerPoint.

Quantification and statistical analyses

Numbers of biological samples were reported in each experimental comparison. For human tissue immunostaining quantifications, percentages of PCs expressing a specific marker were determined from 6 to 10 independent microscopic fields, averaged and reported for each patient sample. For mouse tissue staining quantifications, numbers or percentages of positive stained cells were determined from specific region of interest (e.g., crypt or crypt-villus axis) and averaged for each field. Values of at least five independent fields were reported for each animal of a number of animals reported in each comparison group. All graphic data and statistical analyses were conducted using GraphPad Prism 9 (https://www.graphpad.com) and Microsoft Excel Office 365. The data were reported as mean ± SEM. Statistical comparisons for two groups was performed by unpaired Student's *t*-test, and for multiple groups was performed by one-way or two-way ANOVA.

Data availability

The single cell RNA-Seq datasets are available in Gene Expression Omnibus (GEO) with an accession number: GSE237329 (http://www.ncbi.nlm.nih.gov/geo/query/acc.cgi?acc=GSE237329). The bulk RNA sequencing datasets are available as GSE237101 (http://www.ncbi.nlm.nih.gov/geo/query/acc.cgi?acc=GSE237101).

Expanded View for this article is available online.

Acknowledgements
The authors thank Tammy Mui-Galenkamp at Rutgers-NJMS Flow Cytometry Core for helping with FACS analysis, Patricia Soteropoulos, Mainul Hoque, Neeraja Syed, and Seema Hussain at Rutgers Genomics Center for their help with scRNA sequencing, Peter Romanienko and Ghassan Yehia at Rutgers Genome Editing Core Facility for developing the Lyz1$^{3'UTR\text{-}CreER}$ mice. We thank Dr. Daniel Laubitz, Dr. Gabriele Schiro, and Mrs. Anna Williams at the PANDA Core for Genomics and Microbiome Research at the Steele Children's Research Center, University of Arizona, for their assistance with microbiome analysis. This work was supported by the NIH grants R01 DK102934, R01 DK119198, R21 AI167079 and R01 AT010243, NSF/BIO/IDBR grants (1353890, 1952823), ACS Scholar Award (RSG-15-060-01-TBE), and a Rutgers IMRT award to NG; NIH grants R01 DK125296 and R01 DK124274 to TCL; NCI R37CA277821 and NSF IIS-2128307 to LZ; Rutgers University Chancellor's SEED Grant to EMB; the NSF grants IOS-1456673 and IOS-1754783 to RPF; NIH R35GM142702 to WVL; grants of NHLBI HL154757-01A1 and NIAID AI143256-01A1 to YZ; NIH F31 DK121428 to SB; NJDOH/NJ Commission on Cancer Research DCHS19PPC038 to JF, COCR24PRF017 to JBS, and a CCFA Career Development Award Ref. 406794 to SY.

Author contributions
Iyshwarya Balasubramanian: Conceptualization; data curation; formal analysis; validation; investigation; methodology; writing – original draft. **Sheila Bandyopadhyay:** Data curation; formal analysis; investigation; methodology; writing – original draft; writing – review and editing. **Juan Flores:** Formal analysis; investigation; methodology. **Jared Bianchi-Smak:** Formal analysis; investigation; methodology. **Xiang Lin:** Formal analysis; validation; investigation; methodology. **Haoran Liu:** Formal analysis; investigation. **Shengxiang Sun:** Formal analysis; investigation. **Natasha B Golovchenko:** Resources; investigation. **Yue Liu:** Formal analysis; investigation; methodology. **Dahui Wang:** Formal analysis; investigation. **Radha Patel:** Investigation. **Ivor Joseph:** Investigation; methodology. **Panan Suntornsaratoon:** Formal analysis; investigation. **Justin Vargas:** Resources. **Peter HR Green:** Resources. **Govind Bhagat:** Resources. **Stephen M Lagana:** Resources. **Wang Ying:** Formal analysis. **Yi Zhang:** Resources; investigation; methodology. **Zhihan Wang:** Resources; investigation; methodology. **Wei Vivian Li:** Formal analysis; investigation. **Sukhwinder Singh:** Investigation; methodology. **Zhongren Zhou:** Resources. **George Kollias:** Resources. **Laura A Farr:** Resources; investigation. **Shannon N Moonah:** Resources. **Shiyan Yu:** Resources; investigation. **Zhi Wei:** Supervision; methodology. **Edward M Bonder:** Supervision; investigation; methodology. **Lanjing Zhang:** Formal analysis; supervision; investigation; methodology. **Pawel R Kiela:** Supervision; investigation; methodology. **Karen L Edelblum:** Resources; supervision. **Ronaldo Ferraris:** Supervision; funding acquisition; investigation. **Ta-Chiang Liu:** Conceptualization; formal analysis; supervision; funding acquisition; validation; investigation; methodology; writing – original draft; writing – review and editing. **Nan Gao:** Conceptualization; resources; data curation; formal analysis; supervision; funding acquisition; validation; investigation; visualization; methodology; writing – original draft; project administration; writing – review and editing.

Disclosure and competing interests statement
The authors declare that they have no conflict of interest.

References

Adachi O, Kawai T, Takeda K, Matsumoto M, Tsutsui H, Sakagami M, Nakanishi K, Akira S (1998) Targeted disruption of the MyD88 gene results in loss of IL-1- and IL-18-mediated function. *Immunity* 9: 143–150

Adolph TE, Tomczak MF, Niederreiter L, Ko HJ, Bock J, Martinez-Naves E, Glickman JN, Tschurtschenthaler M, Hartwig J, Hosomi S *et al* (2013) Paneth cells as a site of origin for intestinal inflammation. *Nature* 503: 272–276

Almohazey D, Lo YH, Vossler CV, Simmons AJ, Hsieh JJ, Bucar EB, Schumacher MA, Hamilton KE, Lau KS, Shroyer NF *et al* (2017) The ErbB3 receptor tyrosine kinase negatively regulates Paneth cells by PI3K-dependent suppression of Atoh1. *Cell Death Differ* 24: 855–865

Alzoghaibi MA, Al-Mofleh IA, Al-Jebreen AM (2008) Neutrophil chemokines GCP-2 and GRO-alpha in patients with inflammatory bowel disease. *J Dig Dis* 9: 144–148

Arijs I, De Hertogh G, Lemaire K, Quintens R, Van Lommel L, Van Steen K, Leemans P, Cleynen I, Van Assche G, Vermeire S *et al* (2009) Mucosal gene expression of antimicrobial peptides in inflammatory bowel disease before and after first infliximab treatment. *PLoS One* 4: e7984

Ashida N, Arai H, Yamasaki M, Kita T (2001) Differential signaling for MCP-1-dependent integrin activation and chemotaxis. *Ann NY Acad Sci* 947: 387–389

Barthel M, Hapfelmeier S, Quintanilla-Martinez L, Kremer M, Rohde M, Hogardt M, Pfeffer K, Russmann H, Hardt WD (2003) Pretreatment of mice with streptomycin provides a *Salmonella enterica* serovar Typhimurium colitis model that allows analysis of both pathogen and host. *Infect Immun* 71: 2839–2858

Batlle E, Henderson JT, Beghtel H, van den Born MM, Sancho E, Huls G, Meeldijk J, Robertson J, van de Wetering M, Pawson T *et al* (2002) Beta-catenin and TCF mediate cell positioning in the intestinal epithelium by controlling the expression of EphB/ephrinB. *Cell* 111: 251–263

Bedini OA, Naves A, San Miguel P, Quispe A, Guida C (2014) Metaplasic Paneth cells in ulcerative colitis. *Acta Gastroenterol Latinoam* 44: 285–289

Begun J, Lassen KG, Jijon HB, Baxt LA, Goel G, Heath RJ, Ng A, Tam JM, Kuo SY, Villablanca EJ *et al* (2015) Integrated genomics of Crohn's disease risk variant identifies a role for CLEC12A in antibacterial autophagy. *Cell Rep* 11: 1905–1918

Bel S, Pendse M, Wang Y, Li Y, Ruhn KA, Hassell B, Leal T, Winter SE, Xavier RJ, Hooper LV (2017) Paneth cells secrete lysozyme via secretory autophagy during bacterial infection of the intestine. *Science* 357: 1047–1052

Benjamin JL, Sumpter R Jr, Levine B, Hooper LV (2013) Intestinal epithelial autophagy is essential for host defense against invasive bacteria. *Cell Host Microbe* 13: 723–734

Bevins CL, Salzman NH (2011) Paneth cells, antimicrobial peptides and maintenance of intestinal homeostasis. *Nat Rev Microbiol* 9: 356–368

Bikoff EK, Huang LY, Episkopou V, van Meerwijk J, Germain RN, Robertson EJ (1993) Defective major histocompatibility complex class II assembly, transport, peptide acquisition, and $CD4^+$ T cell selection in mice lacking invariant chain expression. *J Exp Med* 177: 1699–1712

Biton M, Haber AL, Rogel N, Burgin G, Beyaz S, Schnell A, Ashenberg O, Su CW, Smillie C, Shekhar K *et al* (2018) T helper cell cytokines modulate intestinal stem cell renewal and differentiation. *Cell* 175: 1307–1320

Blidberg K, Palmberg L, Dahlén B, Lantz A-S, Larsson K (2012) Chemokine release by neutrophils in chronic obstructive pulmonary disease. *Innate Immun* 18: 503–510

Borghese F, Clanchy FI (2011) CD74: an emerging opportunity as a therapeutic target in cancer and autoimmune disease. *Expert Opin Ther Targets* 15: 237–251

Bozic CR, Kolakowski LF Jr, Gerard NP, Garcia-Rodriguez C, von Uexkull-Guldenband C, Conklyn MJ, Breslow R, Showell HJ, Gerard C (1995) Expression and biologic characterization of the murine chemokine KC. *J Immunol* 154: 6048–6057

Bozzi F, Mogavero A, Varinelli L, Belfiore A, Manenti G, Caccia C, Volpi CC, Beznoussenko GV, Milione M, Leoni V *et al* (2017) MIF/CD74 axis is a target for novel therapies in colon carcinomatosis. *J Exp Clin Cancer Res* 36: 16

Bucala R, Shachar I (2014) The integral role of CD74 in antigen presentation, MIF signal transduction, and B cell survival and homeostasis. *Mini Rev Med Chem* 14: 1132–1138

Buczacki SJ, Zecchini HI, Nicholson AM, Russell R, Vermeulen L, Kemp R, Winton DJ (2013) Intestinal label-retaining cells are secretory precursors expressing Lgr5. *Nature* 495: 65–69

Burns K, Martinon F, Esslinger C, Pahl H, Schneider P, Bodmer JL, Di Marco F, French L, Tschopp J (1998) MyD88, an adapter protein involved in interleukin-1 signaling. *J Biol Chem* 273: 12203–12209

Butler A, Hoffman P, Smibert P, Papalexi E, Satija R (2018) Integrating single-cell transcriptomic data across different conditions, technologies, and species. *Nat Biotechnol* 36: 411–420

Cadwell K, Liu JY, Brown SL, Miyoshi H, Loh J, Lennerz JK, Kishi C, Kc W, Carrero JA, Hunt S *et al* (2008) A key role for autophagy and the autophagy gene Atg16l1 in mouse and human intestinal Paneth cells. *Nature* 456: 259–263

Cadwell K, Patel KK, Maloney NS, Liu TC, Ng AC, Storer CE, Head RD, Xavier R, Stappenbeck TS, Virgin HW (2010) Virus-plus-susceptibility gene interaction determines Crohn's disease gene Atg16L1 phenotypes in intestine. *Cell* 141: 1135–1145

Callahan BJ, McMurdie PJ, Rosen MJ, Han AW, Johnson AJ, Holmes SP (2016) DADA2: high-resolution sample inference from Illumina amplicon data. *Nat Methods* 13: 581–583

Caporaso JG, Lauber CL, Walters WA, Berg-Lyons D, Huntley J, Fierer N, Owens SM, Betley J, Fraser L, Bauer M *et al* (2012) Ultra-high-throughput microbial community analysis on the Illumina HiSeq and MiSeq platforms. *ISME J* 6: 1621–1624

Ceder JA, Jansson L, Helczynski L, Abrahamsson PA (2008) Delta-like 1 (Dlk-1), a novel marker of prostate basal and candidate epithelial stem cells, is downregulated by notch signalling in intermediate/transit amplifying cells of the human prostate. *Eur Urol* 54: 1344–1353

Chang JY, Antonopoulos DA, Kalra A, Tonelli A, Khalife WT, Schmidt TM, Young VB (2008) Decreased diversity of the fecal microbiome in recurrent *Clostridium difficile*-associated diarrhea. *J Infect Dis* 197: 435–438

Chassaing B, Aitken JD, Malleshappa M, Vijay-Kumar M (2014) Dextran sulfate sodium (DSS)-induced colitis in mice. *Curr Protoc Immunol* 104: 15.25.1–15.25.14

Chu FF, Doroshow JH, Esworthy RS (1993) Expression, characterization, and tissue distribution of a new cellular selenium-dependent glutathione peroxidase, GSHPx-GI. *J Biol Chem* 268: 2571–2576

Chu F-F, Esworthy RS, Doroshow JH (2004) Role of Se-dependent glutathione peroxidases in gastrointestinal inflammation and cancer. *Free Radic Biol Med* 36: 1481–1495

Coelho AL, Schaller MA, Benjamim CF, Orlofsky AZ, Hogaboam CM, Kunkel SL (2007) The chemokine CCL6 promotes innate immunity via immune cell activation and recruitment. *J Immunol* 179: 5474–5482

Collins T, Korman AJ, Wake CT, Boss JM, Kappes DJ, Fiers W, Ault KA, Gimbrone MA, Strominger JL, Pober JS (1984) Immune interferon activates multiple class II major histocompatibility complex genes and the associated invariant chain gene in human endothelial cells and dermal fibroblasts. *Proc Natl Acad Sci USA* 81: 4917–4921

Comerford I, Harata-Lee Y, Bunting MD, Gregor C, Kara EE, McColl SR (2013) A myriad of functions and complex regulation of the CCR7/CCL19/CCL21 chemokine axis in the adaptive immune system. *Cytokine Growth Factor Rev* 24: 269–283

Cunliffe RN (2003) Alpha-defensins in the gastrointestinal tract. *Mol Immunol* 40: 463–467

Cunliffe RN, Rose FR, Keyte J, Abberley L, Chan WC, Mahida YR (2001) Human defensin 5 is stored in precursor form in normal Paneth cells and is expressed by some villous epithelial cells and by metaplastic Paneth cells in the colon in inflammatory bowel disease. *Gut* 48: 176–185

Darmoul D, Ouellette AJ (1996) Positional specificity of defensin gene expression reveals Paneth cell heterogeneity in mouse small intestine. *Am J Physiol* 271: G68–G74

Di Sabatino A, Miceli E, Dhaliwal W, Biancheri P, Salerno R, Cantoro L, Vanoli A, De Vincenzi M, Blanco Cdel V, MacDonald TT *et al* (2008) Distribution, proliferation, and function of Paneth cells in uncomplicated and complicated adult celiac disease. *Am J Clin Pathol* 130: 34–42

Diehl GE, Longman RS, Zhang JX, Breart B, Galan C, Cuesta A, Schwab SR, Littman DR (2013) Microbiota restricts trafficking of bacteria to mesenteric lymph nodes by CX_3CR1^{hi} cells. *Nature* 494: 116–120

Donato KA, Gareau MG, Wang YJJ, Sherman PM (2010) *Lactobacillus rhamnosus* GG attenuates interferon-γ and tumour necrosis factor-α-induced barrier dysfunction and pro-inflammatory signalling. *Microbiology* 156: 3288–3297

Doron S, Snydman DR, Gorbach SL (2005) Lactobacillus GG: bacteriology and clinical applications. *Gastroenterol Clin North Am* 34: 483–498

Duerkop BA, Vaishnava S, Hooper LV (2009) Immune responses to the microbiota at the intestinal mucosal surface. *Immunity* 31: 368–376

Farin HF, Karthaus WR, Kujala P, Rakhshandehroo M, Schwank G, Vries RG, Kalkhoven E, Nieuwenhuis EE, Clevers H (2014) Paneth cell extrusion and release of antimicrobial products is directly controlled by immune cell-derived IFN-gamma. *J Exp Med* 211: 1393–1405

Farr L, Ghosh S, Jiang N, Watanabe K, Parlak M, Bucala R, Moonah S (2020a) CD74 signaling links inflammation to intestinal epithelial cell regeneration and promotes mucosal healing. *Cell Mol Gastroenterol Hepatol* 10: 101–112

Farr L, Ghosh S, Moonah S (2020b) Role of MIF cytokine/CD74 receptor pathway in protecting against injury and promoting repair. *Front Immunol* 11: 1273

Feng G, Bajpai G, Ma P, Koenig A, Bredemeyer A, Lokshina I, Lai L, Förster I, Leuschner F, Kreisel D *et al* (2022) CCL17 aggravates myocardial injury by suppressing recruitment of regulatory T cells. *Circulation* 145: 765–782

Fishbein T, Novitskiy G, Mishra L, Matsumoto C, Kaufman S, Goyal S, Shetty K, Johnson L, Lu A, Wang A *et al* (2008) NOD2-expressing bone marrow-derived cells appear to regulate epithelial innate immunity of the transplanted human small intestine. *Gut* 57: 323–330

Fitzgerald KA, Palsson-McDermott EM, Bowie AG, Jefferies CA, Mansell AS, Brady G, Brint E, Dunne A, Gray P, Harte MT *et al* (2001) Mal (MyD88-adapter-like) is required for Toll-like receptor-4 signal transduction. *Nature* 413: 78–83

Fletcher JR, Pike CM, Parsons RJ, Rivera AJ, Foley MH, McLaren MR, Montgomery SA, Theriot CM (2021) *Clostridioides difficile* exploits toxin-mediated inflammation to alter the host nutritional landscape and exclude competitors from the gut microbiota. *Nat Commun* 12: 462

Gao N, Kaestner KH (2010) Cdx2 regulates endo-lysosomal function and epithelial cell polarity. *Genes Dev* 24: 1295–1305

Gaudino SJ, Beaupre M, Lin X, Joshi P, Rathi S, McLaughlin PA, Kempen C, Mehta N, Eskiocak O, Yueh B *et al* (2021) IL-22 receptor signaling in Paneth cells is critical for their maturation, microbiota colonization, Th17-related immune responses, and anti-*Salmonella* immunity. *Mucosal Immunol* 14: 389–401

Gu L, Tseng SC, Rollins BJ (1999) Monocyte chemoattractant protein-1. *Chem Immunol* 72: 7–29

Gulati AS, Shanahan MT, Arthur JC, Grossniklaus E, von Furstenberg RJ, Kreuk L, Henning SJ, Jobin C, Sartor RB (2012) Mouse background strain profoundly influences Paneth cell function and intestinal microbial composition. *PLoS One* 7: e32403

Haber AL, Biton M, Rogel N, Herbst RH, Shekhar K, Smillie C, Burgin G, Delorey TM, Howitt MR, Katz Y *et al* (2017) A single-cell survey of the small intestinal epithelium. *Nature* 551: 333–339

Hall AB, Yassour M, Sauk J, Garner A, Jiang X, Arthur T, Lagoudas GK, Vatanen T, Fornelos N, Wilson R *et al* (2017) A novel *Ruminococcus gnavus* clade enriched in inflammatory bowel disease patients. *Genome Med* 9: 103

He S, Wang J, Kato K, Xie F, Varambally S, Mineishi S, Kuick R, Mochizuki K, Liu Y, Nieves E *et al* (2012) Inhibition of histone methylation arrests ongoing graft-versus-host disease in mice by selectively inducing apoptosis of alloreactive effector T cells. *Blood* 119: 1274–1282

He G-W, Lin L, DeMartino J, Zheng X, Staliarova N, Dayton T, Begthel H, van de Wetering WJ, Bodewes E, van Zon J *et al* (2022) Optimized human intestinal organoid model reveals interleukin-22-dependency of paneth cell formation. *Cell Stem Cell* 29: 1333–1345

Henne C, Schwenk F, Koch N, Moller P (1995) Surface expression of the invariant chain (CD74) is independent of concomitant expression of major histocompatibility complex class II antigens. *Immunology* 84: 177–182

Hou B, Reizis B, DeFranco AL (2008) Toll-like receptors activate innate and adaptive immunity by using dendritic cell-intrinsic and -extrinsic mechanisms. *Immunity* 29: 272–282

Hu K (2021) Become competent in generating RNA-seq heat maps in one day for novices without prior R experience. *Methods Mol Biol* 2239: 269–303

Jones DE, Bevins CL (1992) Paneth cells of the human small intestine express an antimicrobial peptide gene. *J Biol Chem* 267: 23216–23225

Joossens M, Huys G, Cnockaert M, De Preter V, Verbeke K, Rutgeerts P, Vandamme P, Vermeire S (2011) Dysbiosis of the faecal microbiota in patients with Crohn's disease and their unaffected relatives. *Gut* 60: 631–637

Jung YS, Lee HY, Kim SD, Park JS, Kim JK, Suh PG, Bae YS (2013) Wnt5a stimulates chemotactic migration and chemokine production in human neutrophils. *Exp Mol Med* 45: e27

Kamioka M, Goto Y, Nakamura K, Yokoi Y, Sugimoto R, Ohira S, Kurashima Y, Umemoto S, Sato S, Kunisawa J *et al* (2022) Intestinal commensal microbiota and cytokines regulate Fut2^{+} Paneth cells for gut defense. *Proc Natl Acad Sci USA* 119: e2115230119

Karlsson A, Dahlgren C (2002) Assembly and activation of the neutrophil NADPH oxidase in granule membranes. *Antioxid Redox Signal* 4: 49–60

Kazanjian A, Noah T, Brown D, Burkart J, Shroyer NF (2010) Atonal homolog 1 is required for growth and differentiation effects of notch/gamma-secretase inhibitors on normal and cancerous intestinal epithelial cells. *Gastroenterology* 139: 918–928

Kernbauer E, Ding Y, Cadwell K (2014) An enteric virus can replace the beneficial function of commensal bacteria. *Nature* 516: 94–98

Khaloian S, Rath E, Hammoudi N, Gleisinger E, Blutke A, Giesbertz P, Berger E, Metwaly A, Waldschmitt N, Allez M *et al* (2020) Mitochondrial impairment drives intestinal stem cell transition into dysfunctional Paneth cells predicting Crohn's disease recurrence. *Gut* 69: 1939–1951

Kirsebom FCM, Kausar F, Nuriev R, Makris S, Johansson C (2019) Neutrophil recruitment and activation are differentially dependent on MyD88/TRIF and MAVS signaling during RSV infection. *Mucosal Immunol* 12: 1244–1255

Klinke A, Nussbaum C, Kubala L, Friedrichs K, Rudolph TK, Rudolph V, Paust H-J, Schröder C, Benten D, Lau D *et al* (2011) Myeloperoxidase attracts neutrophils by physical forces. *Blood* 117: 1350–1358

Kontoyiannis D, Pasparakis M, Pizarro TT, Cominelli F, Kollias G (1999) Impaired on/off regulation of TNF biosynthesis in mice lacking TNF AU-rich elements: implications for joint and gut-associated immunopathologies. *Immunity* 10: 387–398

Kroeger KM, Sullivan BM, Locksley RM (2009) IL-18 and IL-33 elicit Th2 cytokines from basophils via a MyD88- and p38alpha-dependent pathway. *J Leukoc Biol* 86: 769–778

Kroemer A, Elsabbagh AM, Matsumoto CS, Zasloff M, Fishbein TM (2016) The microbiome and its implications in intestinal transplantation. *Curr Opin Organ Transplant* 21: 135–139

Lawrance IC, Fiocchi C, Chakravarti S (2001) Ulcerative colitis and Crohn's disease: distinctive gene expression profiles and novel susceptibility candidate genes. *Hum Mol Genet* 10: 445–456

Lebeer S, Vanderleyden J, De Keersmaecker SC (2008) Genes and molecules of lactobacilli supporting probiotic action. *Microbiol Mol Biol Rev* 72: 728–764

Leng L, Metz CN, Fang Y, Xu J, Donnelly S, Baugh J, Delohery T, Chen Y, Mitchell RA, Bucala R (2003) MIF signal transduction initiated by binding to CD74. *J Exp Med* 197: 1467–1476

Lessa FC, Mu Y, Bamberg WM, Beldavs ZG, Dumyati GK, Dunn JR, Farley MM, Holzbauer SM, Meek JI, Phipps EC *et al* (2015) Burden of *Clostridium difficile* infection in the United States. *N Engl J Med* 372: 825–834

Levine JE, Huber E, Hammer ST, Harris AC, Greenson JK, Braun TM, Ferrara JL, Holler E (2013) Low Paneth cell numbers at onset of gastrointestinal graft-versus-host disease identify patients at high risk for nonrelapse mortality. *Blood* 122: 1505–1509

Li L, Xu L, Yan J, Zhen ZJ, Ji Y, Liu CQ, Lau WY, Zheng L, Xu J (2015) CXCR2-CXCL1 axis is correlated with neutrophil infiltration and predicts a poor prognosis in hepatocellular carcinoma. *J Exp Clin Cancer Res* 34: 129

Liu TC, Gao F, McGovern DP, Stappenbeck TS (2014) Spatial and temporal stability of paneth cell phenotypes in Crohn's disease: implications for prognostic cellular biomarker development. *Inflamm Bowel Dis* 20: 646–651

Liu TC, Gurram B, Baldridge M, Head R, Lam V, Luo C, Cao Y, Simpson P, Hayward M, Holtz M *et al* (2016) Paneth cell defects in Crohn's disease patients promote dysbiosis. *JCI Insight* 1: e86907

Liu TC, Kern JT, VanDussen KL, Xiong S, Kaiko GE, Wilen CB, Rajala MW, Caruso R, Holtzman MJ, Gao F *et al* (2018) Interaction between smoking and ATG16L1T300A triggers Paneth cell defects in Crohn's disease. *J Clin Invest* 128: 5110–5122

Liu TC, Kern JT, Jain U, Sonnek NM, Xiong S, Simpson KF, VanDussen KL, Winkler ES, Haritunians T, Malique A *et al* (2021) Western diet induces Paneth cell defects through microbiome alterations and farnesoid X receptor and type I interferon activation. *Cell Host Microbe* 29: 988–1001

Luperchio SA, Schauer DB (2001) Molecular pathogenesis of *Citrobacter rodentium* and transmissible murine colonic hyperplasia. *Microbes Infect* 3: 333–340

Luperchio SA, Newman JV, Dangler CA, Schrenzel MD, Brenner DJ, Steigerwalt AG, Schauer DB (2000) *Citrobacter rodentium*, the causative agent of transmissible murine colonic hyperplasia, exhibits clonality: synonymy of *C. rodentium* and mouse-pathogenic *Escherichia coli*. *J Clin Microbiol* 38: 4343–4350

Ma YJ, Garred P (2018) Pentraxins in complement activation and regulation. *Front Immunol* 9: 3046

Madisen L, Zwingman TA, Sunkin SM, Oh SW, Zariwala HA, Gu H, Ng LL, Palmiter RD, Hawrylycz MJ, Jones AR *et al* (2010) A robust and high-throughput Cre reporting and characterization system for the whole mouse brain. *Nat Neurosci* 13: 133–140

Maurer M, von Stebut E (2004) Macrophage inflammatory protein-1. *Int J Biochem Cell Biol* 36: 1882–1886

McDonald LC, Killgore GE, Thompson A, Owens RC Jr, Kazakova SV, Sambol SP, Johnson S, Gerding DN (2005) An epidemic, toxin gene–variant strain of *Clostridium difficile*. *N Engl J Med* 353: 2433–2441

Medzhitov R, Preston-Hurlburt P, Kopp E, Stadlen A, Chen C, Ghosh S, Janeway CA Jr (1998) MyD88 is an adaptor protein in the hToll/IL-1 receptor family signaling pathways. *Mol Cell* 2: 253–258

Meisch JP, Nishimura M, Vogel RM, Sung HC, Bednarchik BA, Ghosh SK, Fu P, McCormick T, Weinberg A, Levine AD (2013) Human beta-defensin 3 peptide is increased and redistributed in Crohn's ileitis. *Inflamm Bowel Dis* 19: 942–953

Mitsuyama K, Tsuruta O, Tomiyasu N, Takaki K, Suzuki A, Masuda J, Yamasaki H, Toyonaga A, Sata M (2006) Increased circulating concentrations of growth-related oncogene (GRO)-alpha in patients with inflammatory bowel disease. *Dig Dis Sci* 51: 173–177

Moine L, Rivoira M, de Barboza GD, Pérez A, de Talamoni NT (2018) Glutathione depleting drugs, antioxidants and intestinal calcium absorption. *World J Gastroenterol* 24: 4979–4988

Momburg F, Koch N, Möller P, Moldenhauer G, Butcher GW, Hämmerling G (1986) Differential expression of Ia and Ia-associated invariant chain in mouse tissues after *in vivo* treatment with IFN-gamma. *J Immunol* 136: 940–948

Nance SC, Yi AK, Re FC, Fitzpatrick EA (2008) MyD88 is necessary for neutrophil recruitment in hypersensitivity pneumonitis. *J Leukoc Biol* 83: 1207–1217

Naujokas MF, Morin M, Anderson MS, Peterson M, Miller J (1993) The chondroitin sulfate form of invariant chain can enhance stimulation of T cell responses through interaction with CD44. *Cell* 74: 257–268

Nguyen GT, Green ER, Mecsas J (2017) Neutrophils to the ROScue: mechanisms of NADPH oxidase activation and bacterial resistance. *Front Cell Infect Microbiol* 7: 373

Nishino K, Nishida A, Inoue R, Kawada Y, Ohno M, Sakai S, Inatomi O, Bamba S, Sugimoto M, Kawahara M (2018) Analysis of endoscopic brush samples identified mucosa-associated dysbiosis in inflammatory bowel disease. *J Gastroenterol* 53: 95–106

Nordenfelt P, Tapper H (2011) Phagosome dynamics during phagocytosis by neutrophils. *J Leukoc Biol* 90: 271–284

Onishi K, Zandstra PW (2015) LIF signaling in stem cells and development. *Development* 142: 2230–2236

Palomino DC, Marti LC (2015) Chemokines and immunity. *Einstein* 13: 469–473

Parikh K, Antanaviciute A, Fawkner-Corbett D, Jagielowicz M, Aulicino A, Lagerholm C, Davis S, Kinchen J, Chen HH, Alham NK (2019) Colonic epithelial cell diversity in health and inflammatory bowel disease. *Nature* 567: 49–55

Patel S, McCormick BA (2014) Mucosal inflammatory response to *Salmonella typhimurium* infection. *Front Immunol* 5: 311

Perminow G, Beisner J, Koslowski M, Lyckander LG, Stange E, Vatn MH, Wehkamp J (2010) Defective paneth cell-mediated host defense in pediatric ileal Crohn's disease. *Am J Gastroenterol* 105: 452–459

Png CW, Linden SK, Gilshenan KS, Zoetendal EG, McSweeney CS, Sly LI, McGuckin MA, Florin TH (2010) Mucolytic bacteria with increased prevalence in IBD mucosa augment *in vitro* utilization of mucin by other bacteria. *Am J Gastroenterol* 105: 2420–2428

Porter EM, Liu L, Oren A, Anton PA, Ganz T (1997) Localization of human intestinal defensin 5 in Paneth cell granules. *Infect Immun* 65: 2389–2395

Price AE, Shamardani K, Lugo KA, Deguine J, Roberts AW, Lee BL, Barton GM (2018) A map of toll-like receptor expression in the intestinal epithelium reveals distinct spatial, cell type-specific, and temporal patterns. *Immunity* 49: 560–575

Quast C, Pruesse E, Yilmaz P, Gerken J, Schweer T, Yarza P, Peplies J, Glockner FO (2013) The SILVA ribosomal RNA gene database project: improved data processing and web-based tools. *Nucleic Acids Res* 41: D590–D596

Rauch I, Deets KA, Ji DX, von Moltke J, Tenthorey JL, Lee AY, Philip NH, Ayres JS, Brodsky IE, Gronert K *et al* (2017) NAIP-NLRC4 inflammasomes coordinate intestinal epithelial cell expulsion with eicosanoid and IL-18 release via activation of caspase-1 and -8. *Immunity* 46: 649–659

Reeves AE, Theriot CM, Bergin IL, Huffnagle GB, Schloss PD, Young VB (2011) The interplay between microbiome dynamics and pathogen dynamics in a murine model of *Clostridium difficile* infection. *Gut Microbes* 2: 145–158

Reinecker H-C, Loh EY, Ringler DJ, Mehta A, Rombeau JL, MacDermott RP (1995) Monocyte-chemoattractant protein 1 gene expression in intestinal epithelial cells and inflammatory bowel disease mucosa. *Gastroenterology* 108: 40–50

Riedel DD, Kaufmann SH (1997) Chemokine secretion by human polymorphonuclear granulocytes after stimulation with Mycobacterium tuberculosis and lipoarabinomannan. *Infect Immun* 65: 4620–4623

Rubio CA (2011) Lysozyme-rich mucus metaplasia in duodenal crypts supersedes Paneth cells in celiac disease. *Virchows Arch* 459: 339–346

Rubio CA (2015) Increased production of lysozyme associated with bacterial proliferation in Barrett's esophagitis, chronic gastritis, gluten-induced atrophic duodenitis (celiac disease), lymphocytic colitis, collagenous colitis, ulcerative colitis and Crohn's colitis. *Anticancer Res* 35: 6365–6372

Rumio C, Besusso D, Palazzo M, Selleri S, Sfondrini L, Dubini F, Ménard S, Balsari A (2004) Degranulation of paneth cells via toll-like receptor 9. *Am J Pathol* 165: 373–381

Salzman NH, Chou MM, de Jong H, Liu L, Porter EM, Paterson Y (2003a) Enteric *Salmonella* infection inhibits Paneth cell antimicrobial peptide expression. *Infect Immun* 71: 1109–1115

Salzman NH, Ghosh D, Huttner KM, Paterson Y, Bevins CL (2003b) Protection against enteric salmonellosis in transgenic mice expressing a human intestinal defensin. *Nature* 422: 522–526

Salzman NH, Hung K, Haribhai D, Chu H, Karlsson-Sjoberg J, Amir E, Teggatz P, Barman M, Hayward M, Eastwood D *et al* (2010) Enteric defensins are essential regulators of intestinal microbial ecology. *Nat Immunol* 11: 76–83

Schafer FQ, Buettner GR (2001) Redox environment of the cell as viewed through the redox state of the glutathione disulfide/glutathione couple. *Free Radic Biol Med* 30: 1191–1212

Schroder B (2016) The multifaceted roles of the invariant chain CD74—more than just a chaperone. *Biochim Biophys Acta* 1863: 1269–1281

Schwartz V, Lue H, Kraemer S, Korbiel J, Krohn R, Ohl K, Bucala R, Weber C, Bernhagen J (2009) A functional heteromeric MIF receptor formed by CD74 and CXCR4. *FEBS Lett* 583: 2749–2757

Segers ME, Lebeer S (2014) Towards a better understanding of *Lactobacillus rhamnosus* GG - host interactions. *Microb Cell Fact* 13: S7

Shi X, Leng L, Wang T, Wang W, Du X, Li J, McDonald C, Chen Z, Murphy JW, Lolis E *et al* (2006) CD44 is the signaling component of the macrophage migration inhibitory factor-CD74 receptor complex. *Immunity* 25: 595–606

Simmonds N, Furman M, Karanika E, Phillips A, Bates AW (2014) Paneth cell metaplasia in newly diagnosed inflammatory bowel disease in children. *BMC Gastroenterol* 14: 93

Singh R, Balasubramanian I, Zhang L, Gao N (2020) Metaplastic Paneth cells in extra-intestinal mucosal niche indicate a link to microbiome and inflammation. *Front Physiol* 11: 280

Spalinger MR, Rogler G, Scharl M (2014) Crohn's disease: loss of tolerance or a disorder of autophagy? *Dig Dis* 32: 370–377

Stockinger B, Pessara U, Lin RH, Habicht J, Grez M, Koch N (1989) A role of Ia-associated invariant chains in antigen processing and pressentation. *Cell* 56: 683–689

Stockinger S, Albers T, Duerr CU, Menard S, Putsep K, Andersson M, Hornef MW (2014) Interleukin-13-mediated paneth cell degranulation and antimicrobial peptide release. *J Innate Immun* 6: 530–541

Street K, Risso D, Fletcher RB, Das D, Ngai J, Yosef N, Purdom E, Dudoit S (2018) Slingshot: cell lineage and pseudotime inference for single-cell transcriptomics. *BMC Genomics* 19: 477

Stuart T, Butler A, Hoffman P, Hafemeister C, Papalexi E, Mauck WM 3rd, Hao Y, Stoeckius M, Smibert P, Satija R (2019) Comprehensive integration of single-cell data. *Cell* 177: 1888–1902

Stzepourginski I, Nigro G, Jacob JM, Dulauroy S, Sansonetti PJ, Eberl G, Peduto L (2017) $CD34^+$ mesenchymal cells are a major component of the intestinal stem cells niche at homeostasis and after injury. *Proc Natl Acad Sci USA* 114: E506–E513

Takahashi N, Vanlaere I, de Rycke R, Cauwels A, Joosten LA, Lubberts E, van den Berg WB, Libert C (2008) IL-17 produced by Paneth cells drives TNF-induced shock. *J Exp Med* 205: 1755–1761

Tanaka M, Saito H, Kusumi T, Fukuda S, Shimoyama T, Sasaki Y, Suto K, Munakata A, Kudo H (2001) Spatial distribution and histogenesis of colorectal Paneth cell metaplasia in idiopathic inflammatory bowel disease. *J Gastroenterol Hepatol* 16: 1353–1359

Tecchio C, Cassatella MA (2016) Neutrophil-derived chemokines on the road to immunity. *Semin Immunol* 28: 119–128

Thachil E, Hugot JP, Arbeille B, Paris R, Grodet A, Peuchmaur M, Codogno P, Barreau F, Ogier-Denis E, Berrebi D *et al* (2012) Abnormal activation of autophagy-induced crinophagy in Paneth cells from patients with Crohn's disease. *Gastroenterology* 142: 1097–1099

Tian T, Zhang J, Lin X, Wei Z, Hakonarson H (2021) Model-based deep embedding for constrained clustering analysis of single cell RNA-seq data. *Nat Commun* 12: 1873

Tsiouris A, Neale JA, Reickert CA, Times M (2012) *Clostridium difficile* of the ileum following total abdominal colectomy, with or without proctectomy: who is at risk? *Dis Colon Rectum* 55: 424–428

Vaishnava S, Behrendt CL, Ismail AS, Eckmann L, Hooper LV (2008) Paneth cells directly sense gut commensals and maintain homeostasis at the intestinal host-microbial interface. *Proc Natl Acad Sci USA* 105: 20858–20863

Vaishnava S, Yamamoto M, Severson KM, Ruhn KA, Yu X, Koren O, Ley R, Wakeland EK, Hooper LV (2011) The antibacterial lectin RegIIIgamma promotes the spatial segregation of microbiota and host in the intestine. *Science* 334: 255–258

van Beelen Granlund A, Østvik AE, Brenna Ø, Torp SH, Gustafsson BI, Sandvik AK (2013) REG gene expression in inflamed and healthy colon mucosa explored by *in situ* hybridisation. *Cell Tissue Res* 352: 639–646

VanderVen BC, Yates RM, Russell DG (2009) Intraphagosomal measurement of the magnitude and duration of the oxidative burst. *Traffic* 10: 372–378

VanDussen KL, Liu TC, Li D, Towfic F, Modiano N, Winter R, Haritunians T, Taylor KD, Dhall D, Targan SR *et al* (2014) Genetic variants synthesize to produce paneth cell phenotypes that define subtypes of Crohn's disease. *Gastroenterology* 146: 200–209

Volc-Platzer B, Majdic O, Knapp W, Wolff K, Hinterberger W, Lechner K, Stingl G (1984) Evidence of HLA-DR antigen biosynthesis by human keratinocytes in disease. *J Exp Med* 159: 1784–1789

Vong L, Lorentz RJ, Assa A, Glogauer M, Sherman PM (2014) Probiotic *Lactobacillus rhamnosus* inhibits the formation of neutrophil extracellular traps. *J Immunol* 192: 1870–1877

Wang Q, Garrity GM, Tiedje JM, Cole JR (2007) Naive Bayesian classifier for rapid assignment of rRNA sequences into the new bacterial taxonomy. *Appl Environ Microbiol* 73: 5261–5267

Wang W, Li Y, Guo X (2020a) A mouse model of *Citrobacter rodentium* oral infection and evaluation of innate and adaptive immune responses. *STAR Protoc* 1: 100218

Wang Y, Song W, Wang J, Wang T, Xiong X, Qi Z, Fu W, Yang X, Chen YG (2020b) Single-cell transcriptome analysis reveals differential nutrient absorption functions in human intestine. *J Exp Med* 217: e20191130

Ward M, Ferguson A, Eastwood MA (1979) Jejunal lysozyme activity and the Paneth cell in coeliac disease. *Gut* 20: 55–58

Wehkamp J, Stange EF (2020) An update review on the Paneth cell as key to ileal Crohn's disease. *Front Immunol* 11: 646

Wehkamp J, Fellermann K, Herrlinger KR, Bevins CL, Stange EF (2005a) Mechanisms of Disease: defensins in gastrointestinal diseases. *Nat Clin Pract Gastroenterol Hepatol* 2: 406–415

Wehkamp J, Salzman NH, Porter E, Nuding S, Weichenthal M, Petras RE, Shen B, Schaeffeler E, Schwab M, Linzmeier R *et al* (2005b) Reduced Paneth cell alpha-defensins in ileal Crohn's disease. *Proc Natl Acad Sci USA* 102: 18129–18134

Wickham H (2016) *ggplot2: elegant graphics for data analysis*. New York, NY: Springer

Wiles S, Clare S, Harker J, Huett A, Young D, Dougan G, Frankel G (2004) Organ specificity, colonization and clearance dynamics *in vivo* following oral challenges with the murine pathogen *Citrobacter rodentium*. *Cell Microbiol* 6: 963–972

Willing BP, Dicksved J, Halfvarson J, Andersson AF, Lucio M, Zheng Z, Järnerot G, Tysk C, Jansson JK, Engstrand L (2010) A pyrosequencing study in twins shows that gastrointestinal microbial profiles vary with inflammatory bowel disease phenotypes. *Gastroenterology* 139: 1844–1854

Wilson CL, Heppner KJ, Rudolph LA, Matrisian LM (1995) The metalloproteinase matrilysin is preferentially expressed by epithelial cells in a tissue-restricted pattern in the mouse. *Mol Biol Cell* 6: 851–869

Winner M, Meier J, Zierow S, Rendon BE, Crichlow GV, Riggs R, Bucala R, Leng L, Smith N, Lolis E *et al* (2008) A novel, macrophage migration inhibitory factor suicide substrate inhibits motility and growth of lung cancer cells. *Cancer Res* 68: 7253–7257

Winter SE, Thiennimitr P, Winter MG, Butler BP, Huseby DL, Crawford RW, Russell JM, Bevins CL, Adams LG, Tsolis RM *et al* (2010) Gut inflammation provides a respiratory electron acceptor for *Salmonella*. *Nature* 467: 426–429

Witte K, Witte E, Sabat R, Wolk K (2010) IL-28A, IL-28B, and IL-29: promising cytokines with type I interferon-like properties. *Cytokine Growth Factor Rev* 21: 237–251

Yan F, Polk DB (2002) Probiotic bacterium prevents cytokine-induced apoptosis in intestinal epithelial cells. *J Biol Chem* 277: 50959–50965

Ying J, Srivastava G, Hsieh WS, Gao Z, Murray P, Liao SK, Ambinder R, Tao Q (2005) The stress-responsive gene GADD45G is a functional tumor suppressor, with its response to environmental stresses frequently disrupted epigenetically in multiple tumors. *Clin Cancer Res* 11: 6442–6449

Yokoi Y, Nakamura K, Yoneda T, Kikuchi M, Sugimoto R, Shimizu Y, Ayabe T (2019) Paneth cell granule dynamics on secretory responses to bacterial stimuli in enteroids. *Sci Rep* 9: 2710

Yu S, Nie Y, Knowles B, Sakamori R, Stypulkowski E, Patel C, Das S, Douard V, Ferraris RP, Bonder EM *et al* (2014) TLR sorting by Rab11 endosomes maintains intestinal epithelial-microbial homeostasis. *EMBO J* 33: 1882–1895

Yu S, Tong K, Zhao Y, Balasubramanian I, Yap GS, Ferraris RP, Bonder EM, Verzi MP, Gao N (2018) Paneth cell multipotency induced by notch activation following injury. *Cell Stem Cell* 23: 46–59

Yu S, Balasubramanian I, Laubitz D, Tong K, Bandyopadhyay S, Lin X, Flores J, Singh R, Liu Y, Macazana C *et al* (2020) Paneth cell-derived lysozyme defines the composition of mucolytic microbiota and the inflammatory tone of the intestine. *Immunity* 53: 398–416

Zasloff M (2002) Antimicrobial peptides of multicellular organisms. *Nature* 415: 389–395

Zhang Y, Louboutin JP, Zhu J, Rivera AJ, Emerson SG (2002) Preterminal host dendritic cells in irradiated mice prime $CD8^+$ T cell-mediated acute graft-versus-host disease. *J Clin Invest* 109: 1335–1344

Zhang Y, Sandy AR, Wang J, Radojcic V, Shan GT, Tran IT, Friedman A, Kato K, He S, Cui S *et al* (2011) Notch signaling is a critical regulator of allogeneic $CD4^+$ T-cell responses mediating graft-versus-host disease. *Blood* 117: 299–308

Zhang Q, Pan Y, Yan R, Zeng B, Wang H, Zhang X, Li W, Wei H, Liu Z (2015) Commensal bacteria direct selective cargo sorting to promote symbiosis. *Nat Immunol* 16: 918–926

Zhu Y, Sun Z, Han Q, Liao L, Wang J, Bian C, Li J, Yan X, Liu Y, Shao C *et al* (2009) Human mesenchymal stem cells inhibit cancer cell proliferation by secreting DKK-1. *Leukemia* 23: 925–933